Electronic Supplementary Information

Enzymolysis-Induced Energy Transfer Co-Assembled System for Spontaneously Recoverable Supramolecular Dynamic Memory

Xuanyu Wang[‡], Zhao Gao[‡,] and Wei Tian**

Shaanxi Key Laboratory of Macromolecular Science and Technology, Xi'an Key Laboratory of Hybrid Lumines-cent Materials and Photonic Device, MOE Key Laboratory of Material Physics and Chemistry under Extraordinary Conditions, School of Chemistry and Chemical Engineering, Northwestern Polytechnical University, Xi'an 710072, P. R. China. E-mail: Zhao Gao (gaozhao@nwpu.edu.cn) and Wei Tian (happytw_3000@nwpu.edu.cn)

Contents

1. Materials and Methods

1,4-diethynylnaphthalene[S1] and 5-iodoisophthalic acid[S2] were synthesized according to the previously reported literatures. Other reagents and solvents used in the experiments were purchased from commercial sources without further purification.

^{1}H NMR and ^{13}C NMR spectra were obtained from Bruker Avance 400 instruments. High-resolution electrospray ionization mass spectra (HR-ESI-MS) were obtained on a Bruker Esquire 3000 plus mass spectrometer equipped with an ESI interface and ion trap analyzer. UV–Vis spectra were performed on a Shimadzu UV-2600 spectrometer. Fluorescence spectra, absolute fluorescence quantum yield (Φ_F) and time-resolved fluorescence lifetime experiments were recorded on an Edinburgh FLS1000 transient steady-state fluorescence spectrometer. Φ_F was measured using a calibrated integrating sphere. Transmission electron microscope (TEM) images were recorded on a FEI Talos F200X electron microscope. SEM experiments were performed on the FEI Verios G4 instrument. PXRD was recorded on a SHIMADZU XRD-7000 with a Cu Kα X-ray source (λ = 1.540598 Å). Dynamic light scattering (DLS) experiments were conducted on a Brookhaven BI-9000AT instrument. All-electron DFT calculations have been carried out by the latest version of ORCA quantum chemistry software (Version 5.0.3).[S3] The BLYP functional and the def2-SVP basis set [S4] were adopted for geometry optimization calculations. The optimal geometry for the complex was determined.

Time-gated logic gate experiment: logic gate devices are assembled according to the corresponding schemes. Wherein the connected PVC hose is fixed in the box as a pathway for the liquid and the output tube as well as the input tubes are placed outside the box. Syringes with different compositions are used as inputs and sample bottle is used as the output of the logic gate. The output is obtained under UV light. The concentrations of **1**, ATP, ALP and dyes in aqueous solution are 1.5×10^{-5} mol L^{-1}, 4.5×10^{-5} mol L^{-1}, 1.0 U/mL and 7.5×10^{-5} mol L^{-1}, respectively.

Supramolecular dynamic memory experiments: customized acrylic plates with cells are used as storage matrix. Photoresistors are placed next to the cells and connect in series with wires to the power supply. Each cell contains **1/ALP/dyes** solution in its initial state. The volume of solution in cell is 1 mL. All cell color and voltage changes are detected under UV light. The concentrations of **1**, ATP, ALP and dyes in aqueous solution are 1.5×10^{-5} mol L^{-1}, 4.5×10^{-5} mol L^{-1}, 1.0 U/mL and 7.5×10^{-5} mol L^{-1}, respectively.

Mathematical fitting of the supramolecular polymerization process: the self-assembly of **1** is described using the solvent-dependent equilibrium model.[S5] The initial conditions of the samples were H_2O/CH_3CN (v:v = 1:999) mixed solvent, and by titrating with the same concentration of good solvent (water) to observe the change in absorption spectra. This model is used to describe the self-assembly of **1** which exhibits a sigmoidal curve as shown in the solvent-dependent UV–Vis experiments, indicating that the transition between self-assemblies and monomers follows an isodesmic mechanism. For the co-assembly of **1** with ATP, a sigmoidal curve is obtained by plotting the fraction of aggregated species versus temperature while monitoring the spectral variation at 406 nm, indicating the involvement of an isodesmic mechanism.[S6]

Calculation of energy transfer properties: the overlap integral (J) is calculated according to the following equation:

$$J(\lambda) = \lambda^4 \times F_D(\lambda) \times \varepsilon_A(\lambda) \quad \text{(Equation. S1)}$$

In this equation, $F_D(\lambda)$ is the fluorescence emission spectrum of donor, while $\varepsilon_A(\lambda)$ is the molar absorption coefficient. λ denotes the wavelength of absorption or emission spectrum. $F_D(\lambda)$ is a dimensionless term in the formula and the value of denominator is normalized to 1 before calculation. Energy transfer efficiency is calculated by following equation [S7]:

$$\Phi_{ET} = 1 - I_{DA}/I_D \quad \text{(Equation. S2)}$$

In this equation, I_{DA} is the intensity of donor emission in presence of acceptor. I_D is the intensity of donor emission in absence of acceptor. Φ_{ET} denotes fractional energy transfer efficiency. Energy transfer rate constant (k_{ET}) under different acceptor loading amounts can be obtained according to the following equation [S7]:

$$k_{ET} = (1/\tau_D)\times(R_0/d)^6 \quad \text{(Equation. S3)}$$

In this equation, τ_D refers to the fluorescence lifetime of donor in the self-assembly state and obtained by measuring the fluorescence lifetime of donor. d stands for the average distance of D/A pair. R_0 Stands for the Fröster radius of D/A pair.

To evaluate light harvesting capability, the antenna effect (AE) of the acceptor is obtained via the following equation [S7]:

$$AE = (I_{DA,\lambda1} - I_{D,\lambda1})/I_{A,\lambda2} \quad \text{(Equation. S4)}$$

In this equation, $I_{DA,\lambda1}$ and $I_{D,\lambda1}$ represent the emission intensity of the donor in the D/A system and the system without acceptor, respectively, when the donor is directly

excited. $I_{A,\ \lambda 2}$ stands for the fluorescence intensity of acceptors when it is directly excited.

Stern-Volmer analysis for energy transfer systems: Two different *Stern-Volmer* equations were used to analyze exciton migration behaviors. For the **1/ATP/PB**, the fluorescence quenching of donor units was analyzed by the following equation [S8]:

$$I_0/I = 1 + K\text{sv} \times [\text{Q}] \qquad \text{(Equation. S5)}$$

In this equation, I_0 and I denote the fluorescence intensity in the absence and presence of acceptor, respectively. [Q] is the acceptor concentration, while K_{sv} is the *Stern-Volmer* constant. For the **1/ATP/EY**, **1/ATP/RhB** and **1/ATP/SR101**, the *Stern-Volmer* plots of I_0/I versus the acceptor concentration deviate from linear tendency. Therefore, we use the modified equation to analyze exciton migration behaviors [S8]:

$$I_0/(I_0 - I) = 1/(f_q \times K_{sv} \times [\text{Q}]) + 1/f_q \qquad \text{(Equation. S6)}$$

In this equation, f_q stands for the percentage of excitons trapped by acceptors during the exciton migration.

Determination of second-order exciton migration rates: According to following supplementary Equations, radiative relaxation and exciton trapping are considered [S9]:

$$\text{D}^* + \text{A} \rightarrow \text{A}^* + \text{D} \text{ (Reaction rate: } k) \qquad \text{(Equation. S7)}$$

$$\text{D}^* \rightarrow \text{D} \text{ (Reaction rate: } k_0) \qquad \text{(Equation. S8)}$$

Accordingly, the quenching rate of exciton can be expressed as follows:

$$d[\text{D}^*]/dt = -k[\text{D}^*][\text{A}] - k_0[\text{D}^*] \qquad \text{(Equation. S9)}$$

Because the excitation power of light source is rather low, it is assumed that the concentration of excited donor is extremely low with respect to that of the ground state acceptor. Hence, the concentration of excitons can be written in the following form:

$$[\text{D}^*] = e^{-1/\tau t} \qquad \text{(Equation. S10)}$$

By plotting the reciprocal of donor fluorescent lifetimes ($1/\tau$) versus the concentration of acceptor, the second-order rate constant for the exciton migration process is equal to the slope of the linearly fitted line.

Determination of number of donors quenched by a single acceptor in energy transfer system: due to both dynamic and static quenching participate in the donor quenching process, a model that combines both mechanisms was used to calculate the *n* value. The expression for the model can be expressed in the following form [S10]:

$$I_F = I_0 + ((I_{lim} - I_0)/(2c_0)) \times ((c_0 + c_a + 1/K_a) - ((c_0 + c_a + 1/K_a)^2 - 4c_0c_a)^{1/2})$$

(Equation. S11)

In this equation, I_F is the observed emission intensity of donor in the D/A system, I_0 is the emission intensity of donor in the absence of acceptor, I_{lim} is the emission intensity of the fully complexed donor (assumed to be zero in the curve fitting), c_0 is the concentration of $(Donor)_n$, and c_a is the concentration of acceptor.

2. Supramolecular self-assembly behaviors of monomer 1

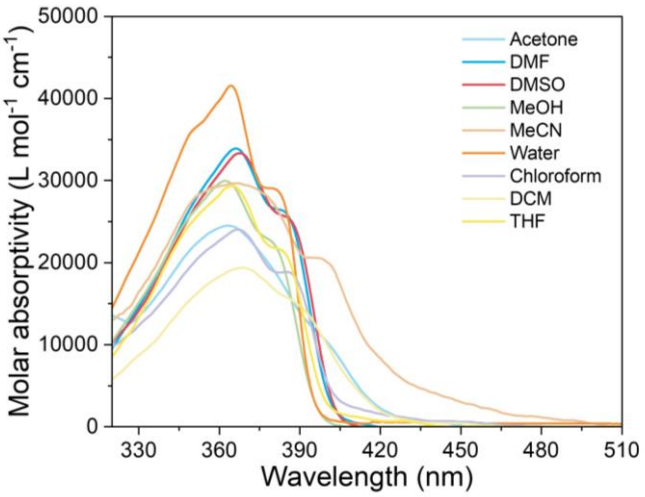

Figure S1. UV-Vis absorption spectra of **1** in various solvents. The concentration of **1** was set at 1.5×10^{-6} mol L^{-1}. We have selected most of the common solvents to study the effect of solvents on the self-assembly of **1**. UV-Vis absorption spectra of **1** in these solvents showed similar absorption bands centered at around 365 nm. In strong polar solvents such as DMF, DMSO, methanol and H_2O, a shoulder peak was observed at around 385 nm, whilst the shoulder peak redshifts to around 400 nm in relatively less polar solvents such as acetone and acetonitrile.

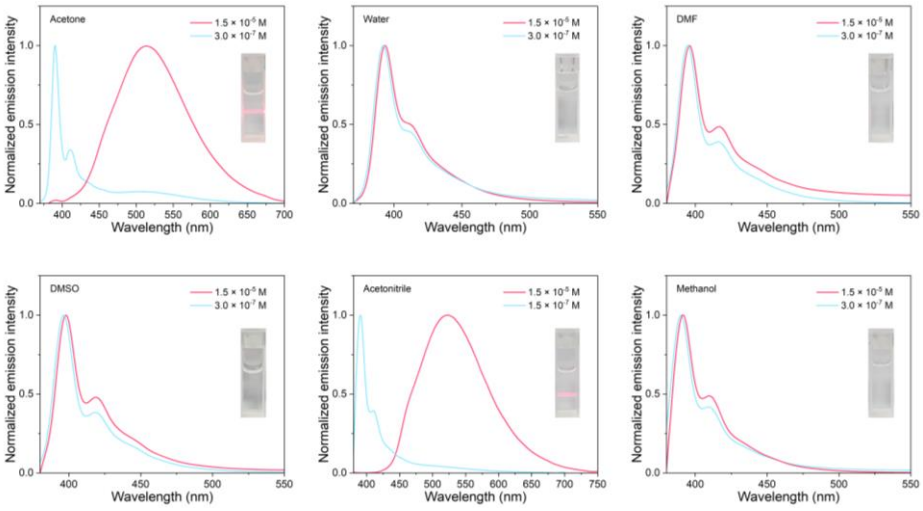

Figure S2. Normalized fluorescence emission spectra of **1** in different solvents. Inset: photograph of Tyndall effect of **1** in different solvents at 1.5×10^{-5} mol L^{-1}. We have selected most of the common solvents to study the effect of solvents on the self-assembly of **1**. Nearly identical fluorescence spectra of **1** in H_2O, DMF, DMSO or methanol between low concentration and high concentration were observed, which proved that monomer **1** possessed relatively good solubility in these solvents. Also, the absence of Tyndall effect verified no formation of large aggregates. However, when the solvent was changed to acetonitrile and acetone, the fluorescence spectra were significantly red-shifted at higher concentration, while a Tyndall effect occurred. These

results undoubtedly indicated the formation of self-assembly **1** in acetonitrile and acetone, while the monomeric state of **1** in H_2O, DMF, DMSO and methanol.

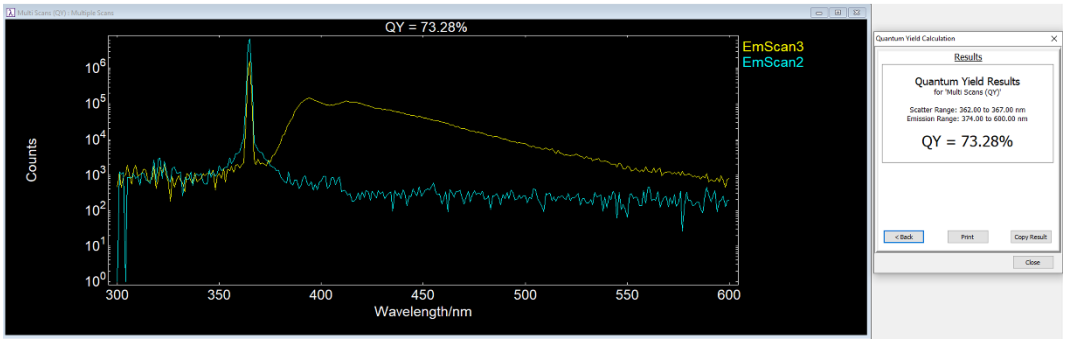

Figure S3. Absolute fluorescence quantum yield of **1** in water.

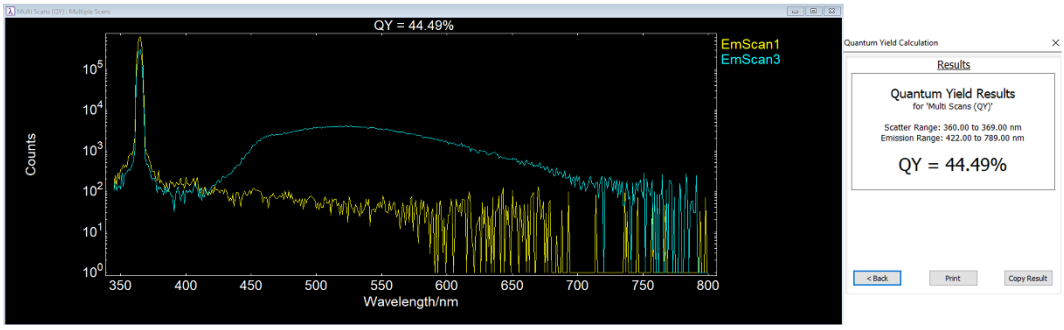

Figure S4. Absolute fluorescence quantum yield of **1** in H_2O/CH_3CN solution (*v: v* = 1: 999).

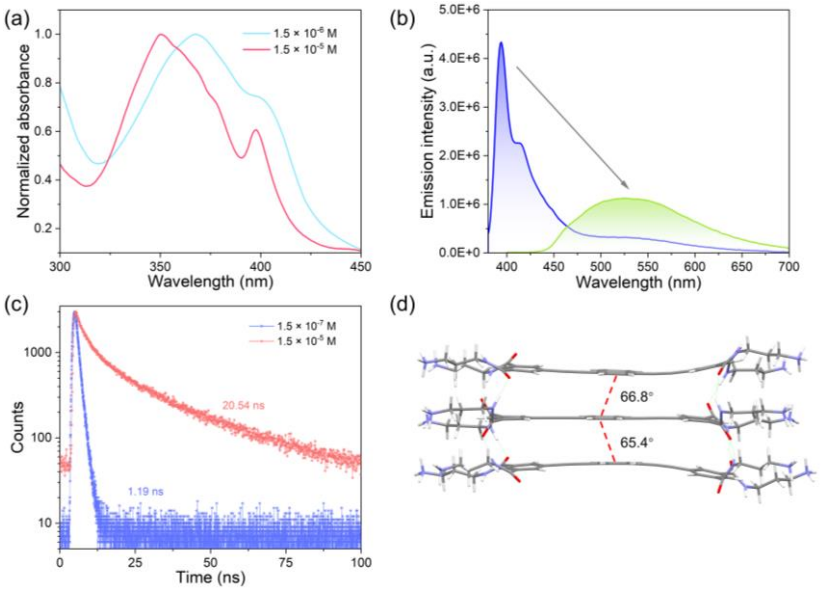

Figure S5. (a) The normalized UV-Vis absorbance spectra of **1** at different concentrations in H_2O/CH_3CN solution (*v* : *v* = 1 : 999). (b) Fluorescence spectra of **1** in pure H_2O (blue line) and H_2O/CH_3CN (green line, *v* : *v* = 1 : 999) solution. The concentration was set at 1.5×10^{-5} mol L^{-1} for both conditions. (c) Fluorescence lifetime

decay profiles of **1** at different concentration in H_2O/CH_3CN solution (v : v = 1:999). (d) Optimized geometries of the trimeric structures of **1** based on DFT calculations. UV-Vis absorption spectrum of **1** in concentrated solution was blue-shifted compared to the highly diluted solution (monomeric state). This is inconsistent with the characteristics of excimer formation, i.e., the excimer should have the same ground state as the monomer and its absorption spectrum should be like that of the monomer. We assumed that the blue-shifted absorption band is more likely attributed to the *H*-aggregation of adjacent naphthalene units. Furthermore, the suppressed and red-shifted fluorescence nature of *H*-aggregation was observed due to the optical forbidden lower excited states. Meanwhile, the increase of the lifetime from 1.19 ns to 20.54 nm was detected. The *H*-aggregation of **1** was further observed by the DFT optimized geometries. The slip angle (θ) of the parallel trimer stacking was calculated to be 66.8° and 65.4°, respectively, which belongs to the *H*-aggregated model (θ>54.7°).

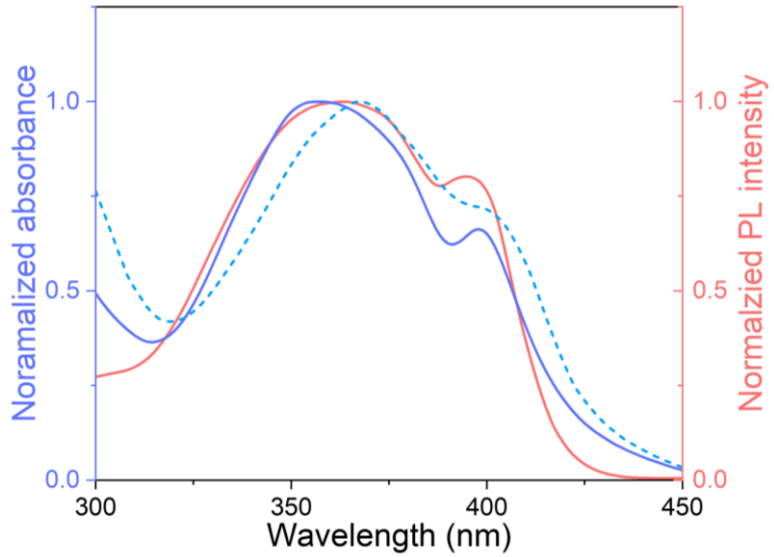

Figure S6. The normalized UV-Vis absorbance spectra of monomer **1** (blue dotted line, 1.5×10^{-6} mol L^{-1}) and self-assembly **1** (blue solid line, 1.5×10^{-5} mol L^{-1}) and fluorescence excitation spectra of self-assembly **1** (pink line, 1.5×10^{-5} mol L^{-1}) at 540 nm in H_2O/CH_3CN solution (v : v = 1 : 999). The excitation spectra of the self-assembly **1** at 540 nm (pink line, 1.5×10^{-5} M) showed a substantial overlap with the UV-vis absorption spectra at the same concentration (blue solid line), but showed a blue shift compared to the monomer **1** (blue dotted line). This phenomenon also confirmed the self-assembly of **1** in the *H*-aggregated manner.

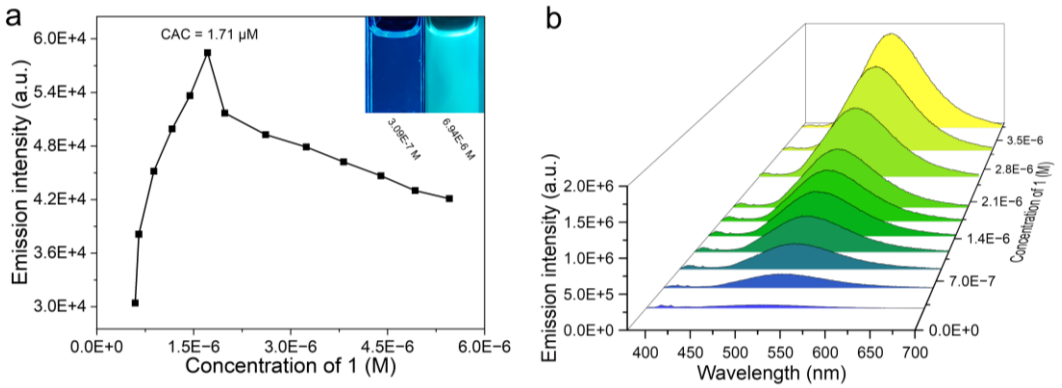

Figure S7. a) The plot of the monomer emission intensity of **1** at 393 nm versus concentration. Inset: the photograph of **1** before and after CAC under 365 nm. b) Concentration-dependent fluorescence spectra of **1** in H_2O/CH_3CN solution (*v*: *v* = 1: 999) from 5.94×10^{-7} M to 3.83×10^{-6} M. λ_{ex} = 365 nm.

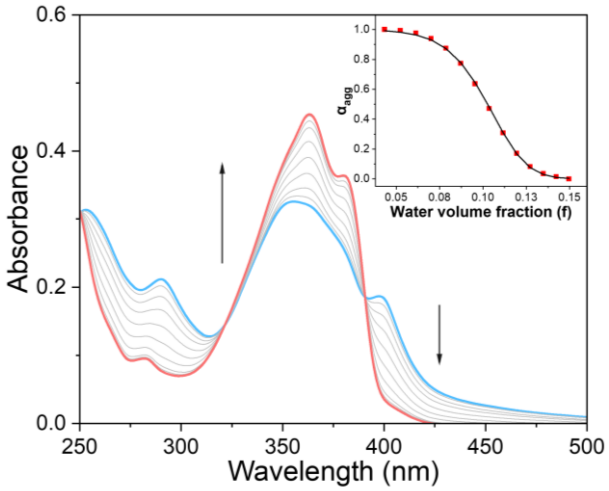

Figure S8. Solvent-dependent UV-Vis spectra of **1** at 1.5×10^{-5} M. Arrows indicate the spectra variations upon increasing the water volume fraction. Inset: α_{agg} of **1** (λ = 400 nm) versus water volume fraction in acetonitrile solution. The red line denotes the isodesmic fitting curve using the solvent-dependent equilibrium model.[S5]

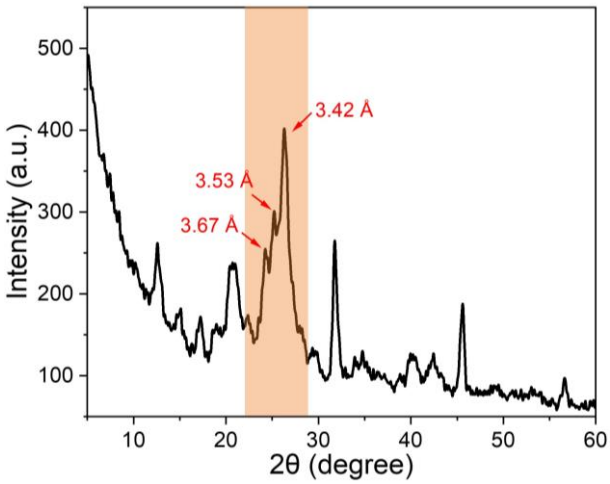

Figure S9. Powder X-ray diffraction pattern of **1**. Diffraction peaks between 22°–29° revealing the existence of π–π stacking.

3. FRET properties of 1 with dyes

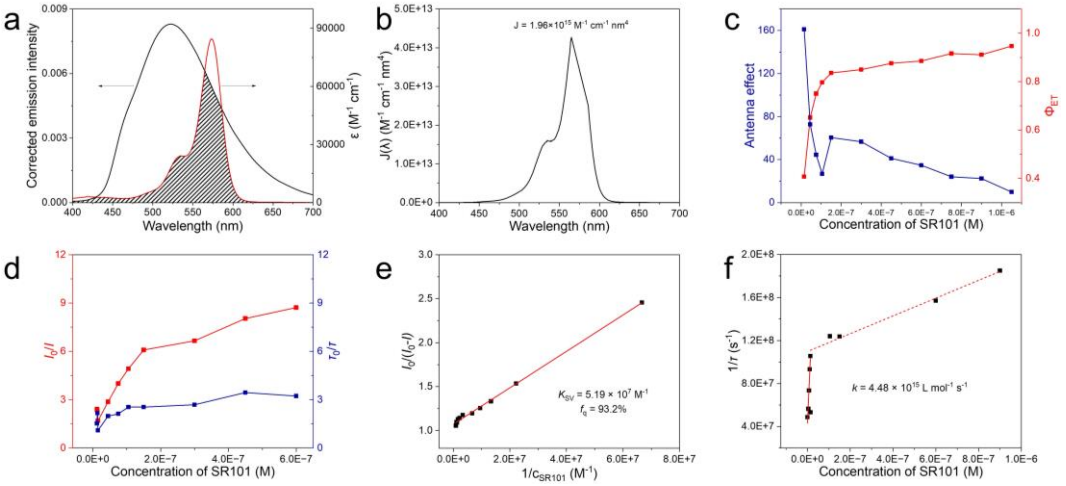

Figure S10. a) The corrected emission spectrum $F_D(\lambda)$ and extinction coefficient spectrum $\varepsilon_A(\lambda)$ of acceptor SR101. b) Spectral overlap between the emission spectra of self-assembly **1** and absorption of SR101. c) Φ_{ET} and antenna effect value of **1/SR101** upon increasing the concentration of the acceptors. d) Stern-Volmer plots of steady-state fluorescence emission and time-resolved fluorescence quenching of **1/SR101**. e) Modified Stern-Volmer plot for fluorescence quenching of **1** in the presence SR101. Through the plotting of $I_0/(I_0 - I)$ versus the reciprocal of the concentration of acceptor, we can obtain K_{sv} and f_q value. The f_q value confirms that how many percentages of excitons are trapped by acceptors. f) Plots of the reciprocal of fluorescence lifetime ($1/\tau$) versus the concentration of SR101. The concentration of **1** is kept at 1.5×10^{-5} mol L^{-1}. Fluorescence lifetimes of **1** are obtained by monitoring the emission at 500 nm.

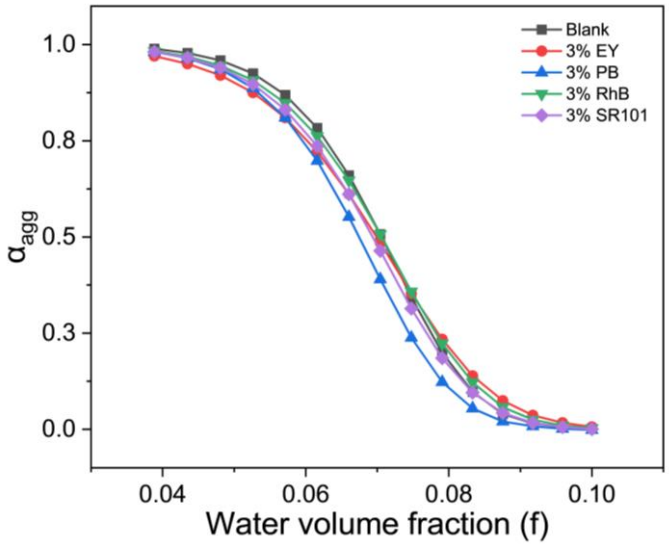

Figure S11. UV-Vis titration fitting curves of self-assembly **1** and **1/EY**, **1/PB**, **1/RhB** as well as **1/SR101**. The curves basically overlap with each other, proving that there is no significant change in the thermodynamic process.

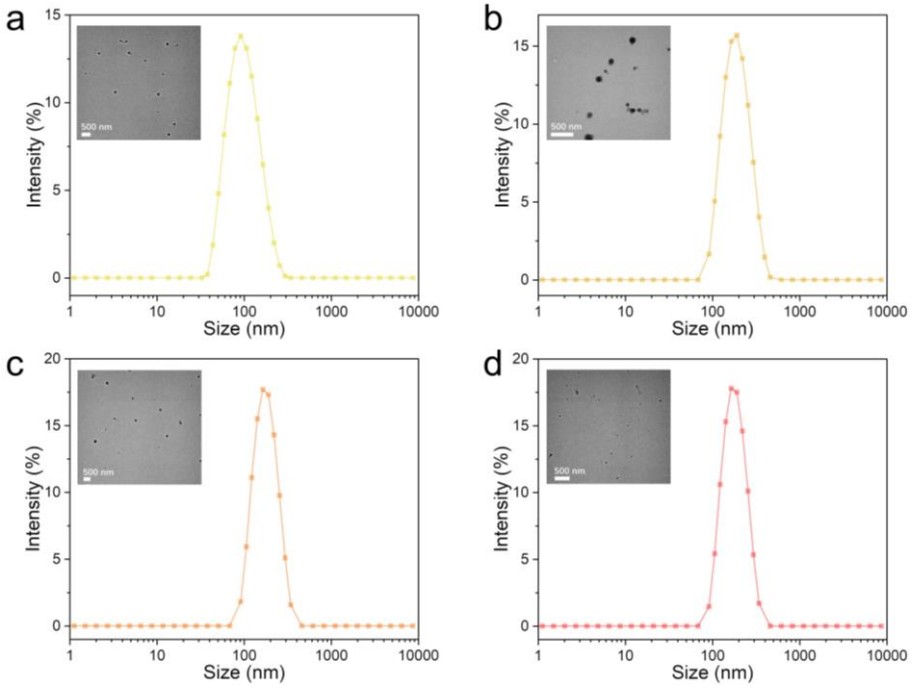

Figure S12. DLS data of a) **1/EY** b) **1/PB** c) **1/RhB** and d) **1/SR101**. Inset: TEM micrograph. The molar ratio of all the dyes to molecule **1** was kept at 3%. It shows no significant difference compared to the self-assembly. Scale bars: 500 nm.

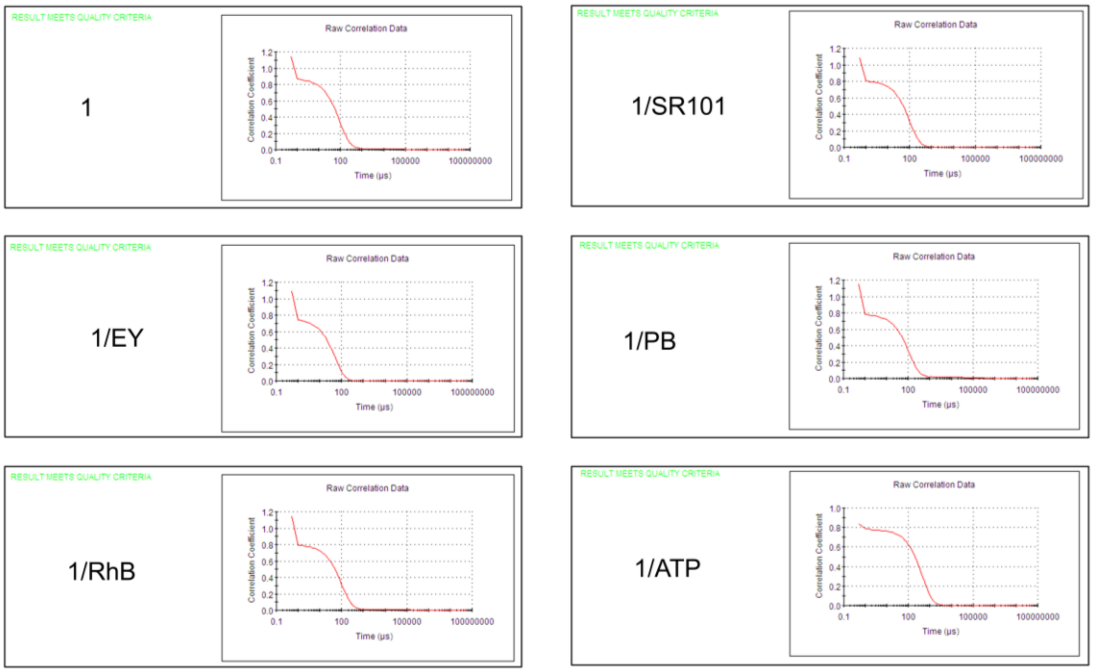

Figure S13. Reliability of DLS experimental results of **1**, **1/EY**, **1/PB**, **1/RhB** and **1/SR101** in H_2O/CH_3CN ($v : v$ = 1 : 999), as well as **1/ATP** in pure water. All the correlation results of DLS met the quality standards, confirming the reliability of these experiments in H_2O/CH_3CN ($v : v$ = 1 : 999).

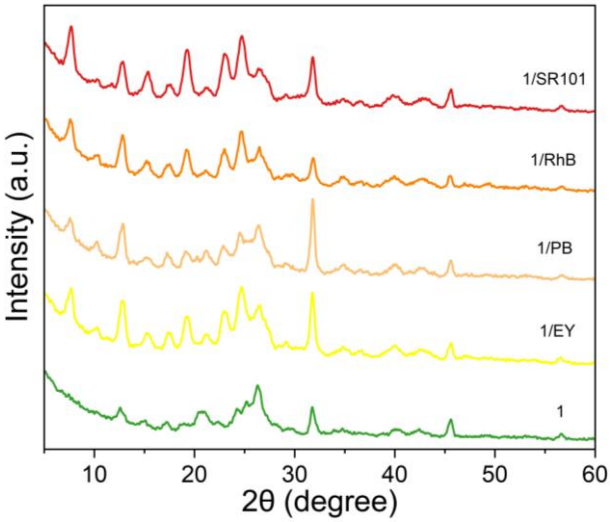

Figure S14. PXRD pattern of **1**, **1/EY**, **1/PB**, **1/RhB** and **1/SR101**. The molar ratio of all the dyes to molecule **1** was kept at 3%. It shows no significant difference compared to the self-assembly.

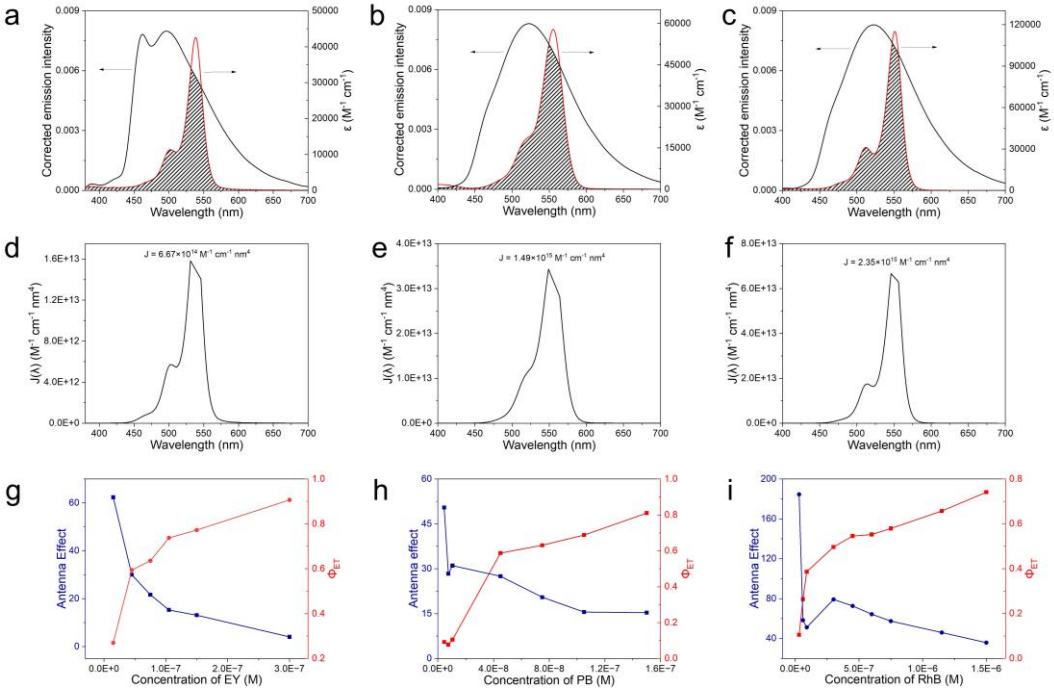

Figure S15. a-c) The corrected emission spectrum $F_D(\lambda)$ and extinction coefficient spectrum $\varepsilon_A(\lambda)$ of acceptor EY, PB and RhB respectively. d-f) Spectral overlap between the emission spectra of **1** and absorption of EY, PB and RhB, respectively. g-i) Φ_{ET} and antenna effect value of **1/EY**, **1/PB** and **1/RhB** upon increasing the concentration of the acceptors, respectively.

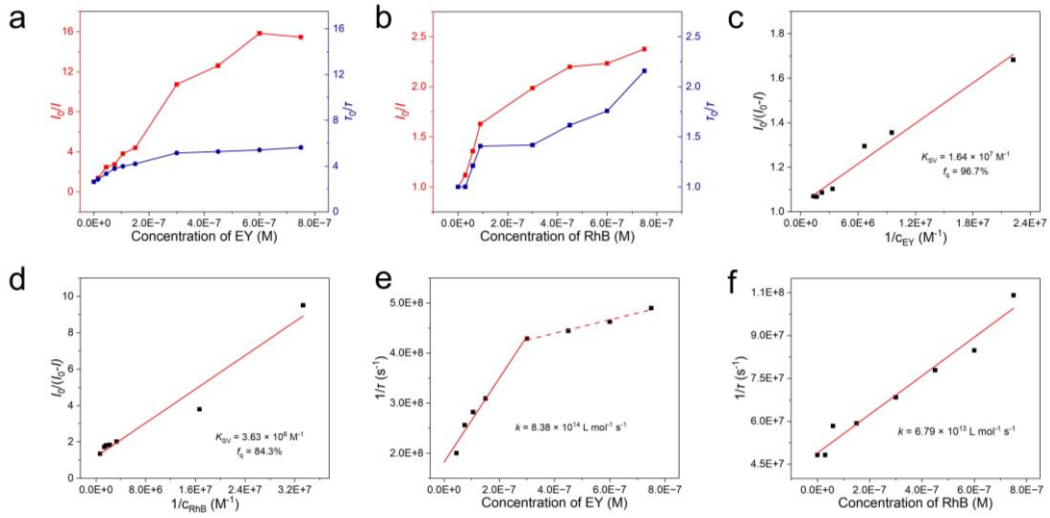

Figure S16. a-b) *Stern-Volmer* plots of steady-state fluorescence emission and time-resolved fluorescence quenching of **1/EY** and **1/RhB**, respectively. c-d) Modified *Stern-Volmer* plot for fluorescence quenching of **1** in the presence of EY and RhB, respectively. e-f) Plots of the reciprocal of fluorescence lifetime ($1/\tau$) versus the concentration of EY and RhB, respectively. The concentration of **1** is kept at 1.5×10^{-5} mol L^{-1}. Fluorescence lifetimes of **1** are obtained by monitoring the emission at 500 nm.

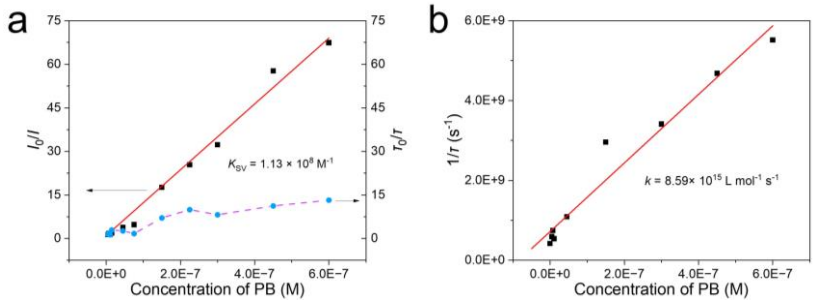

Figure S17. a) *Stern-Volmer* plots of steady-state fluorescence emission and time-resolved fluorescence quenching of **1/PB**. b) Plots of the reciprocal of fluorescence lifetime ($1/\tau$) versus the concentration of PB. The concentration of **1** is kept at 1.5×10^{-5} mol L^{-1}. The fluorescence lifetimes of **1** are obtained by monitoring the emission at 500 nm.

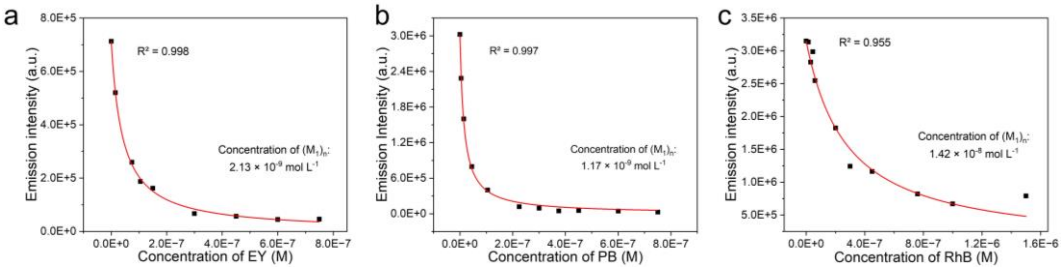

Figure S18. Non-linear fitting of the emission intensity of **1** versus the concentration of a) EY, b) PB and c) RhB. n is the ratio between the concentration of **1** and the concentration of donor matrix 1_n. The concentration of **1** for these experiments was all fixed at 1.5×10^{-5} mol L^{-1}.

Table S1. Fluorescence lifetime decays of **1/EY** upon varying the molar ratios of EY.

Ratio (mol%)	τ_1 (ns)	α_1	τ_2 (ns)	α_2	τ_3 (ns)	α_3	τ_{avg} (ns)	χ^2
0	2.35	42.56%	5.87	27.75%	21.59	29.68%	9.04	1.07
0.10	2.28	58.53%	7.96	26.64%	25.44	14.93%	7.25	1.03
0.50	1.46	51.46%	3.66	33.39%	13.45	15.15%	4.01	1.19
0.70	1.47	62.60%	3.84	26.42%	14.64	10.98%	3.54	1.14
1.00	1.20	46.48%	2.72	39.85%	11.63	13.67%	3.23	1.23
2.00	0.95	59.16%	2.78	32.64%	10.50	8.20%	2.33	1.21
3.00	0.89	59.67%	2.74	32.14%	10.22	8.19%	2.25	1.15
4.00	0.84	56.85%	2.52	34.69%	9.59	8.45%	2.16	1.15
5.00	0.84	57.58%	2.36	32.99%	8.24	9.42%	2.04	1.22

Table S2. Dynamic and static quenching of **1/EY** upon varying the molar ratios of EY.

Ratio (mol%)	k_{ET} (s^{-1})	η_{tot}	η_{dyn}	η_{stat}
0	0	0%	0%	0%
0.10	5.10×10^7	27.0%	19.8%	7.2%
0.50	4.47×10^8	63.6%	56.9%	6.7%
0.70	7.93×10^8	73.8%	60.8%	13.0%
1.00	1.05×10^9	77.2%	64.2%	13.0%
2.00	4.17×10^9	90.7%	74.2%	16.5%
3.00	5.16×10^9	92.1%	75.1%	16.9%
4.00	6.86×10^9	93.7%	76.1%	17.6%
5.00	7.08×10^9	93.5%	77.4%	18.1%

Table S3. Fluorescence lifetime decays of **1/PB** upon varying the molar ratios of PB.

Ratio (mol%)	τ_1 (ns)	α_1	τ_2 (ns)	α_2	τ_3 (ns)	α_3	τ_{avg} (ns)	χ^2
0	1.79	8.36%	6.81	26.17%	28.86	65.47%	20.82	0.99
0.07	1.82	11.05%	6.64	25.94%	26.40	63.01%	18.56	1.07
0.30	1.09	18.04%	4.40	39.30%	16.98	42.66%	9.17	1.04
0.70	1.01	35.50%	3.78	34.81%	15.12	29.69%	6.16	1.25
1.00	0.86	34.09%	3.02	50.07%	9.98	15.84%	3.38	1.25
1.50	0.73	45.71%	2.56	42.06%	8.17	12.23%	2.41	1.23
2.00	0.80	49.44%	2.91	36.99%	9.58	13.57%	2.77	1.22
2.50	0.46	36.23%	1.82	57.10%	8.60	6.67%	1.78	1.19
4.00	0.69	63.68%	2.48	31.81%	10.81	4.52%	1.72	1.19
5.00	0.48	50.08%	1.55	38.36%	4.31	11.57%	1.33	1.23

Table S4. Dynamic and static quenching of **1/PB** upon varying the molar ratios of PB.

Ratio (mol%)	k_{ET} (s^{-1})	η_{tot}	η_{dyn}	η_{stat}
0	0	0%	0%	0%
0.07	5.49×10^6	28.0%	22.4%	5.6%
0.30	8.02×10^7	73.7%	61.6%	12.1%
0.70	5.10×10^8	86.8%	74.2%	12.6%
1.00	1.80×10^9	94.3%	85.9%	8.5%
1.50	2.18×10^9	96.1%	89.9%	6.1%
2.00	3.83×10^9	96.9%	87.7%	9.2%
2.50	8.95×10^9	98.4%	93.2%	5.2%
4.00	9.60×10^9	98.5%	92.4%	6.1%
5.00	2.11×10^{10}	99.1%	94.4%	4.6%

Table S5. Fluorescence lifetime decays of **1/RhB** upon varying the molar ratios of RhB.

Ratio (mol%)	τ_1 (ns)	α_1	τ_2 (ns)	α_2	τ_3 (ns)	α_3	τ_{avg} (ns)	χ^2
0	1.79	8.36%	6.81	26.17%	28.86	65.47%	20.82	0.99
0.20	2.16	10.88%	7.47	25.37%	29.17	63.74%	20.72	1.07
0.40	2.10	19.31%	7.36	25.90%	27.04	54.79%	17.13	0.99
0.60	1.83	22.91%	5.99	26.99%	25.36	50.11%	14.74	1.10
2.00	1.92	14.93%	6.90	31.95%	22.84	53.12%	14.63	1.06
3.00	1.63	17.46%	5.73	34.76%	22.10	47.78%	12.83	1.11
4.00	1.71	24.44%	6.11	32.28%	21.74	43.29%	11.80	1.06
5.00	1.69	31.07%	5.48	31.08	19.50	37.85%	9.61	1.09

Table S6. Dynamic and static quenching of **1/RhB** upon varying the molar ratios of RhB.

Ratio (mol%)	k_{ET} (s^{-1})	η_{tot}	η_{dyn}	η_{stat}
0	0	0%	0%	0%
0.20	2.34×10^6	10.5%	0.1%	10.4%
0.40	8.64×10^6	26.4%	17.4%	8.9%
0.60	1.76×10^7	38.6%	28.9%	9.7%
2.00	2.79×10^7	49.6%	29.5%	20.1%
3.00	3.86×10^7	54.5%	38.1%	16.4%
4.00	4.32×10^7	55.2%	41.1%	12.1%
5.00	5.92×10^7	57.9%	53.7%	4.2%

Table S7. Fluorescence lifetime decays of **1/SR101** upon varying the molar ratios of SR101.

Ratio (mol%)	τ_1 (ns)	α_1	τ_2 (ns)	α_2	τ_3 (ns)	α_3	τ_{avg} (ns)	χ^2
0	1.79	8.36%	6.81	26.17%	28.86	65.47%	20.82	0.99
0.05	1.68	20.08%	5.16	26.65%	22.30	53.26%	13.59	1.08
0.07	1.83	36.47%	6.64	29.52%	23.80	34.01%	10.72	1.04
0.30	1.56	20.39%	5.27	38.18%	19.42	41.42%	10.37	1.07
0.50	1.21	19.20%	4.35	36.54%	17.73	44.26%	9.67	1.03
0.70	1.11	25.15%	3.83	35.02%	16.18	39.82%	8.07	1.26
1.00	1.43	24.93%	5.22	45.41%	18.01	29.55%	8.07	1.22
2.00	1.32	36.36%	5.00	44.14%	17.26	29.50%	7.65	1.09
4.00	1.11	29.05%	4.41	44.36%	15.37	26.59%	6.37	1.09
5.00	0.99	38.64%	3.29	39.74%	11.06	21.62%	4.08	1.21

Table S8. Dynamic and static quenching of **1/SR101** upon varying the molar ratios of SR101.

Ratio (mol%)	k_{ET} (s^{-1})	η_{tot}	η_{dyn}	η_{stat}
0	0	0	0	0
0.05	1.66×10^7	41.8%	33.8%	8.0%
0.07	3.45×10^7	54.1%	47.8%	6.3%
0.30	5.67×10^7	65.2%	49.5%	15.6%
0.50	9.76×10^7	75.0%	52.9%	22.1%
0.70	1.53×10^8	79.7%	60.7%	18.9%
1.00	1.98×10^8	83.6%	60.6%	22.9%
2.00	2.32×10^8	85.0%	62.8%	22.2%
4.00	3.81×10^8	88.5%	69.0%	19.5%
5.00	8.41×10^8	91.6%	80.1%	11.5%

4. Spontaneous fluorochromism in co-assembly 1/ATP

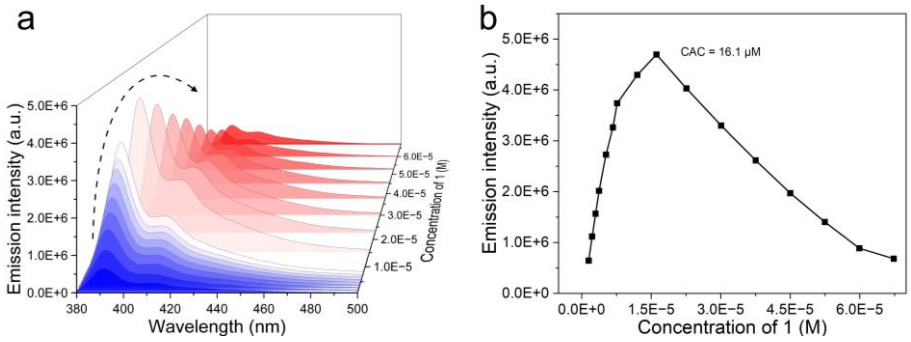

Figure S19. a) Concentration-dependent fluorescence spectra of **1** in aqueous solution from 1.5×10^{-6} M to 6.7×10^{-5} M. λ_{ex} = 365 nm. b) The plot of the emission intensity of **1** at 393 nm versus concentration.

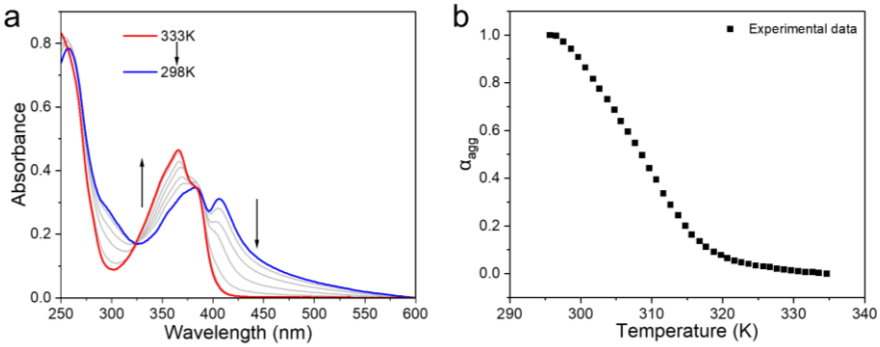

Figure S20. a) Temperature-dependent UV-Vis absorption spectra of **1/ATP** in aqueous solution. b) α_{agg} of **1/ATP** (λ = 406 nm) versus temperature in aqueous solution. The concentration of **1** and ATP was set at 1.5×10^{-5} M and 4.5×10^{-5} M, respectively.

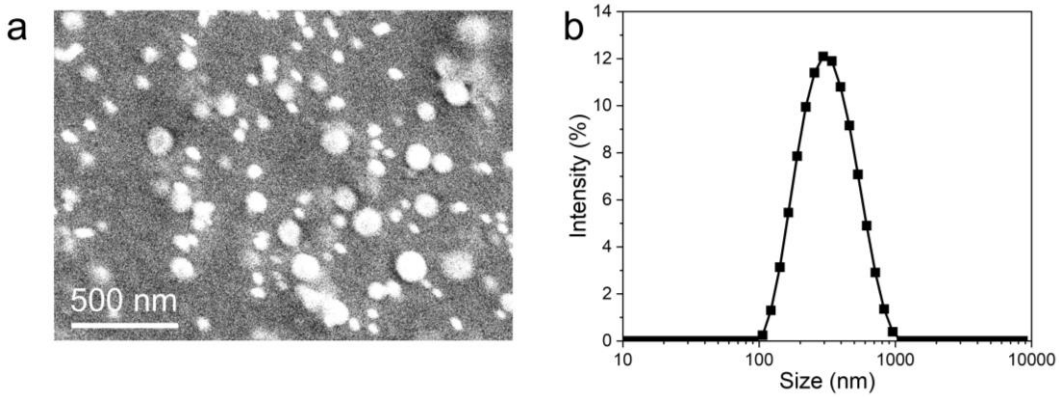

Figure S21. a) SEM micrograph of **1/ATP**. Scale bars: 500 nm. b) DLS curve of the co-assembly of **1/ATP**. The concentration of **1** and ATP is set at 1.5×10^{-5} mol L^{-1} and 4.5×10^{-5} mol L^{-1}, respectively.

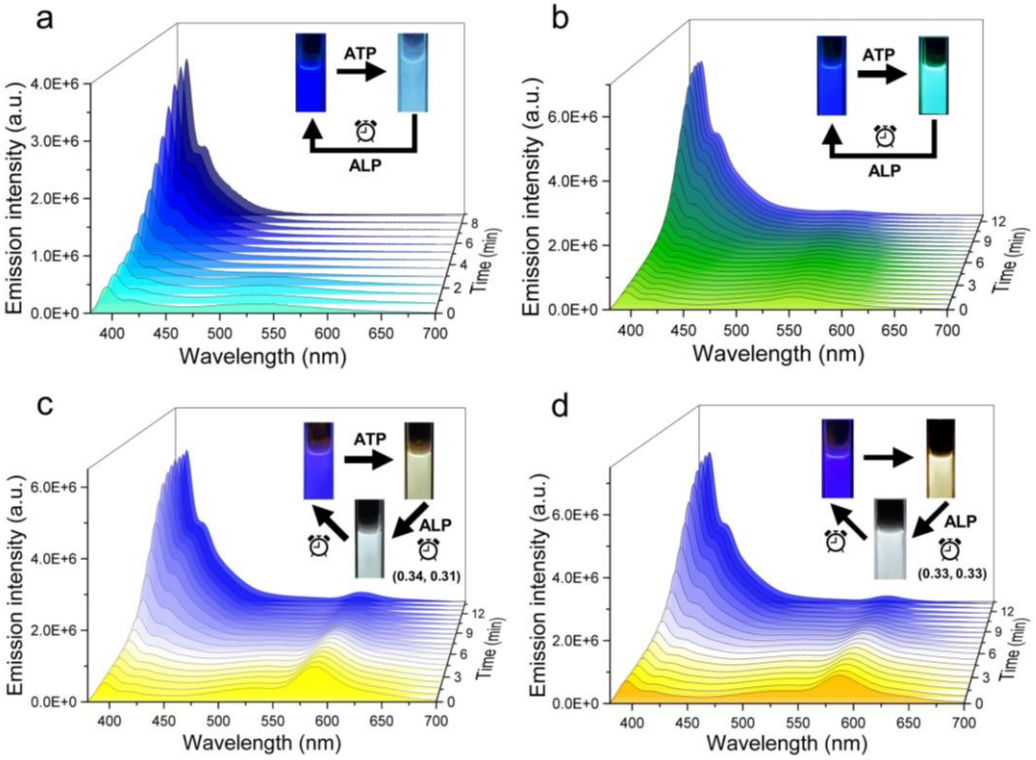

Figure S22. Fluorescence spectra variations of a) **1/ATP**, b) **1/ATP/EY**, c) **1/ATP/PB** and d) **1/ATP/RhB** versus hydrolyzed time in the presence of 1.0 U mL^{-1} of ALP in aqueous solution. λ_{ex} = 365 nm. Inset: photographs before and after hydrolysis under 365 nm excitation.

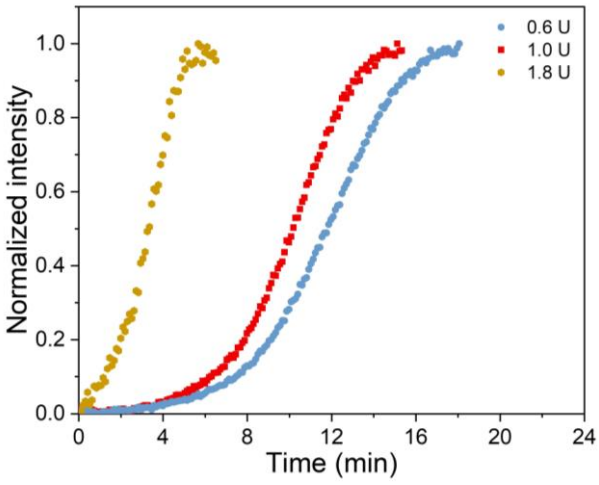

Figure S23. Normalized fluorescence intensity of **1/ATP** (c: 1.5 × 10^{-5} mol L^{-1} for **1** and 4.5 × 10^{-5} mol L^{-1} for ATP) at 393 nm *versus* hydrolyzed time with different concentrations of ALP at 298 K.

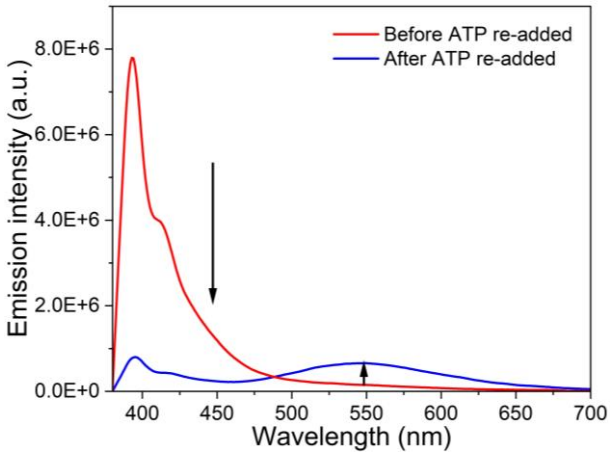

Figure S24. Fluorescence intensity of **1/ATP** (c: 1.5×10^{-5} mol L^{-1} for **1** and 4.5×10^{-5} mol L^{-1} for ATP) before and after re-addition of ATP at 298 K.

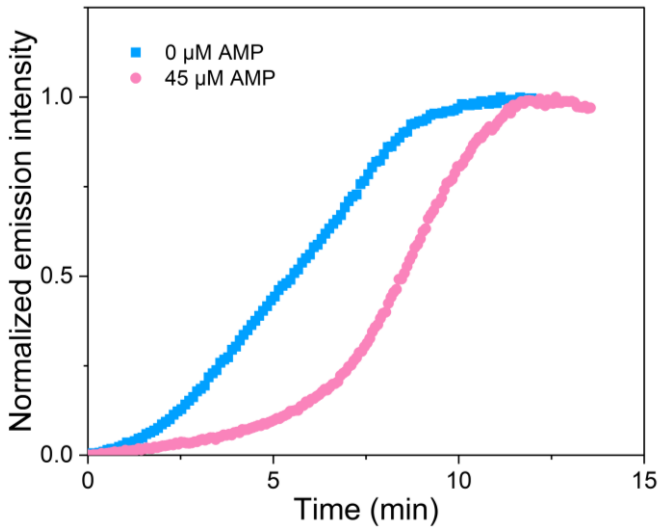

Figure S25. Time-dependent fluorescence intensity of **1/ATP** at 393 nm with and without AMP in the presence of 1.0 U mL^{-1} ALP. The concentration of **1** and ATP were set at 1.5×10^{-5} mol L^{-1} and 4.5×10^{-5} mol L^{-1}, respectively. ALP can hydrolyze ATP to produce AMP. The presence of the hydrolyzed byproduct is known to be a competitive inhibitor of ALP, resulting in a longer hydrolysis time as the number of cycles increases. Thus, by adding AMP in **1/ATP** under 1.0 U mL^{-1} ALP, a slight decrease in the rate of hydrolysis observed. Even so, this waste did not significantly affect the cycling performance of our system. We still maintained good fluorescence reproducibility for at least 6 cycles.

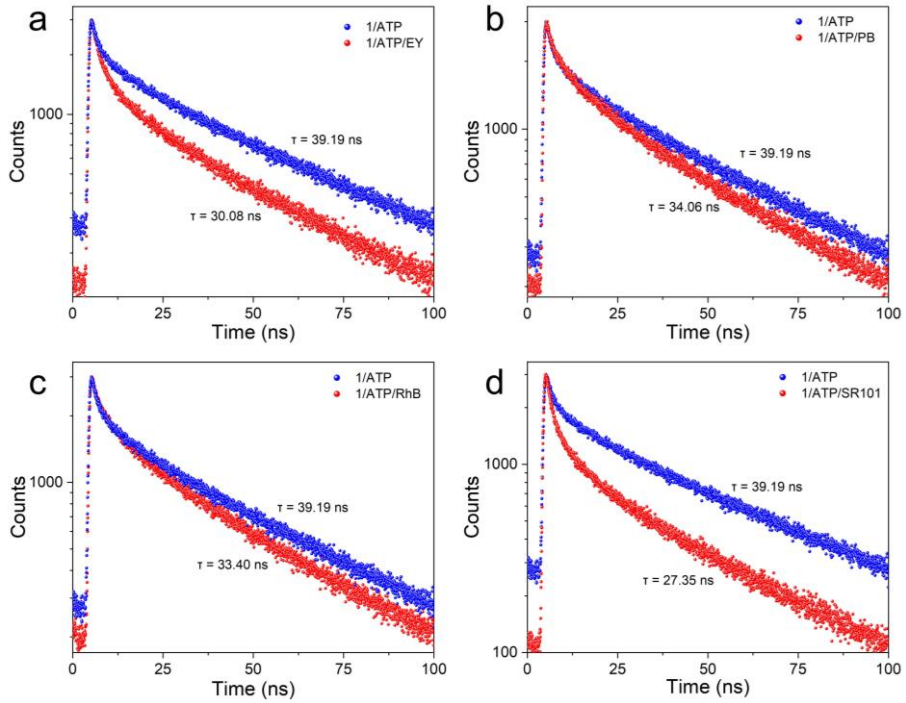

Figure S26. Fluorescence lifetime decay profiles of a) **1/ATP/EY**, b) **1/ATP/PB**, c) **1/ATP/RhB** and d) **1/ATP/SR101**. The concentration is set at 1.5×10^{-5} mol L^{-1} for **1**, 4.5×10^{-5} mol L^{-1} for ATP and 7.5×10^{-7} mol L^{-1} for dyes.

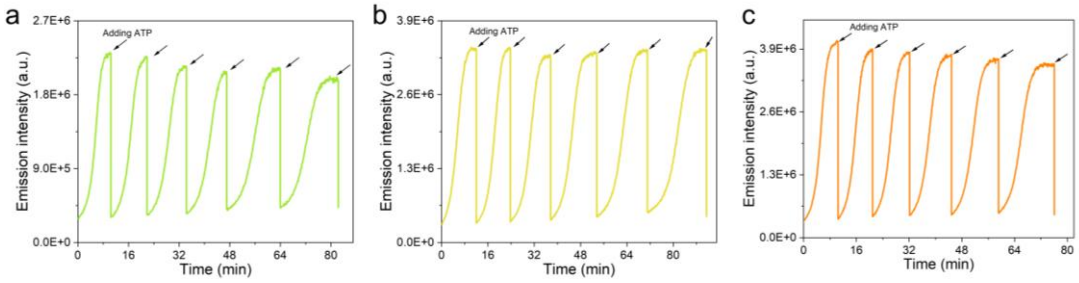

Figure S27. Time-dependent fluorescence intensity at 393 nm upon several repetitive addition of ATP into (a) **1/EY**, (b) **1/PB** and (c) **1/RhB** in the presence of 1.0 U mL^{-1} of ALP. Arrows represent the (re)fuelling points with the addition of ATP ([**1**] = 1.5×10^{-5} mol L^{-1}, [ATP] = 4.5×10^{-5} mol L^{-1}, [EY] = [PB] = [RhB] = 7.5×10^{-7} mol L^{-1}).

5. Spontaneously Recoverable SDM

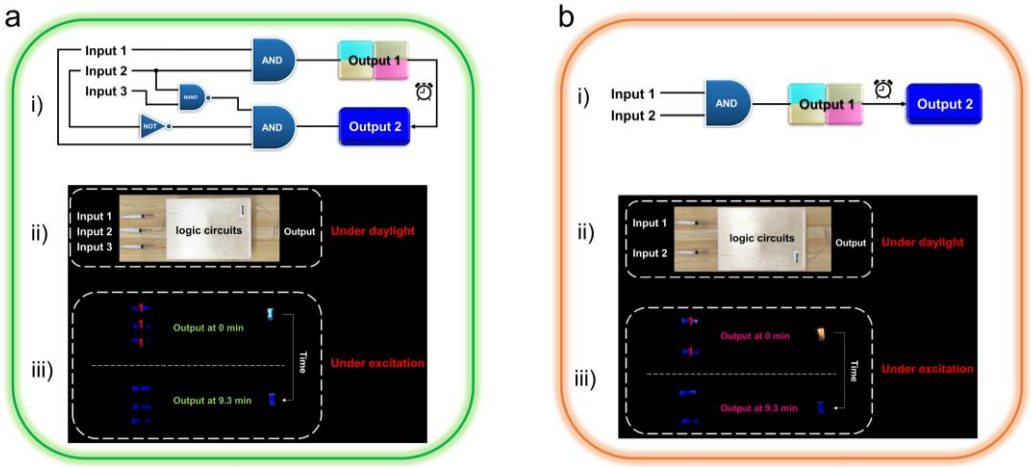

Figure S28. a) i) Scheme of three-input and two-output logic gate. ii) The logic gate device under daylight. iii) The logic gate device under 365 nm excitation using (1, 1, 1) input at 0 min and 9.3 min. b) i) Scheme of two-input and two-output AND logic gate. ii) The logic gate device under daylight. iii) The logic gate device under 365 nm excitation using (1, 1) input at 0 min and 9.3 min.

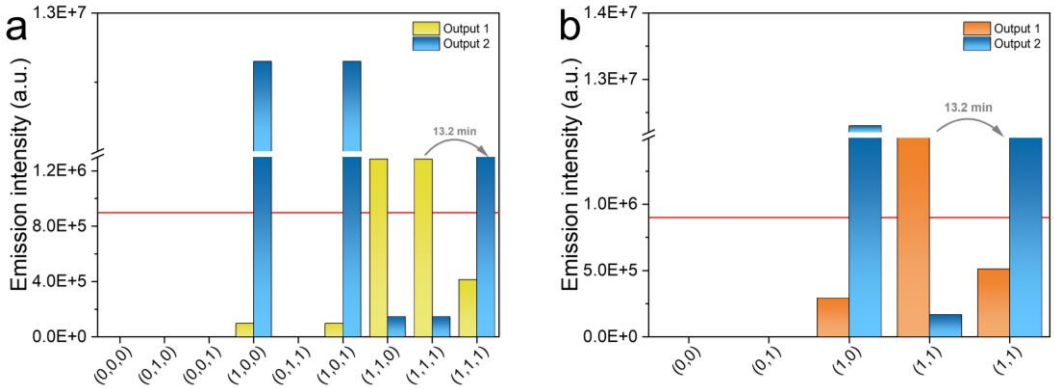

Figure S29. Fluorescence intensity with different inputs combination in the a) EY three-input logic gate system and b) RhB two-input logic gate system. The "false/true" threshold is the red line.

Table S9. The truth tables of four-inputs and two-outputs logic gate.

Input 1	Input 2	Input 3	Input 4	Output 1	Output 2
1	ATP	ALP	SR101	Co-Assembly	Monomer
0	0	0	0	0	0
1	0	0	0	0	1
0	1	0	0	0	0
0	0	0	1	0	0
0	0	1	0	0	0
1	1	0	0	0	0
1	0	0	1	0	1
1	0	1	0	0	1
0	1	0	1	0	0
0	1	1	0	0	0
0	0	1	1	0	0
1	1	0	1	1	0
1	0	1	1	0	1
1	1	1	0	0	1[a]
0	1	1	1	0	0
1	1	1	1	0	1[b]

[a]The output 2 is the change over time from none; [b]The output 2 is the change over time from output 1.

Table S10. The truth tables of three-inputs and two-outputs logic gate.

Input 1	Input 2	Input 3	Output 1	Output 2
1/EY	ATP	ALP	Co-Assembly	Monomer
0	0	0	0	0
1	0	0	0	1
0	1	0	0	0
0	0	1	0	0
1	1	0	1	0
1	0	1	0	1
0	1	1	0	0
1	1	1	0	1[a]

[a]The output 2 is the change over time from output 1.

Table S11. The truth tables of two-inputs and two-outputs logic gate.

Input 1	Input 2	Output 1	Output 2
1/RhB/ALP	ATP	Co-Assembly	Monomer
0	0	0	0
1	0	0	0
0	1	0	0
1	1	0	1[a]

[a]The output 2 is the change over time from output 1.

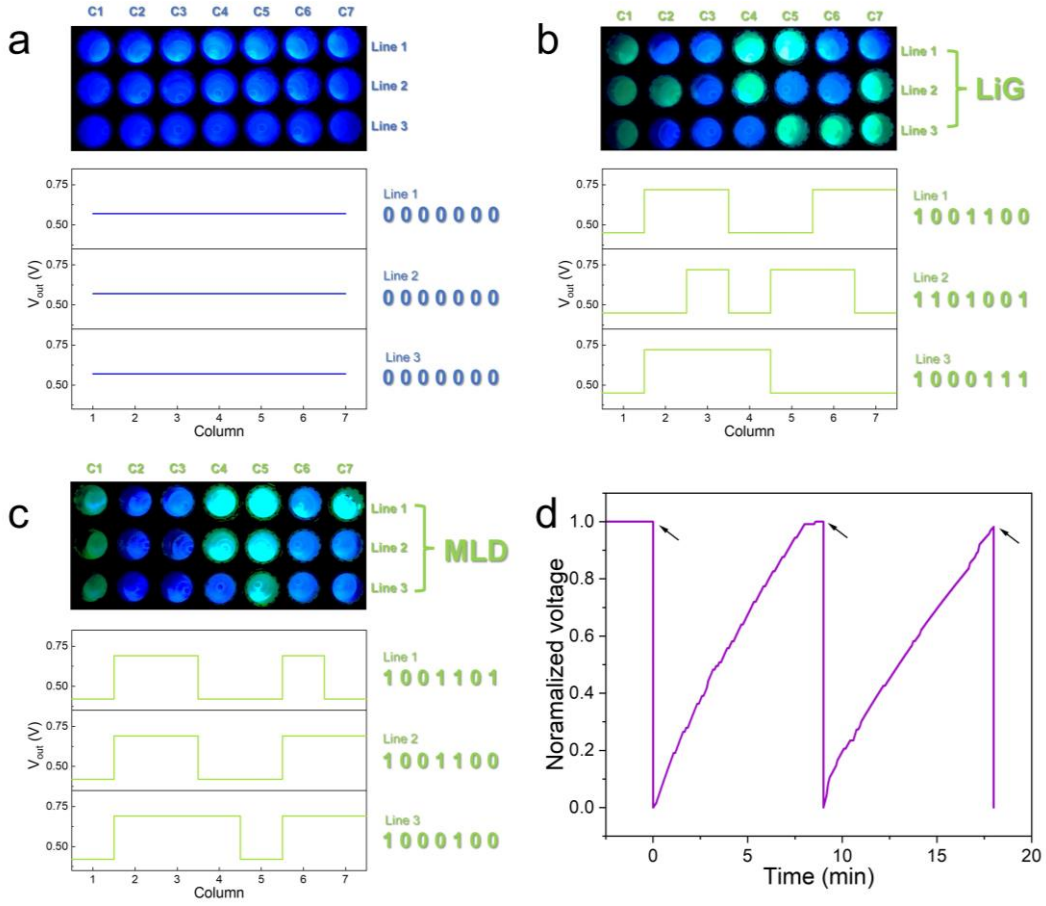

Figure S30. a-c) Storage matrix under 365 nm excitation and the corresponding voltages for each data point. The voltages can be converted into binary code to get the information. d) Time-dependent normalized voltage intensity of single data point upon several repetitive additions of ATP in the presence of 1.0 U mL^{-1} of ALP, respectively. Arrows represent the (re)fuelling points with the addition of ATP. The concentration of **1**, ATP and EY are set at 1.5×10^{-5} mol L^{-1}, 4.5×10^{-5} mol L^{-1} and 7.5×10^{-7} mol L^{-1}, respectively.

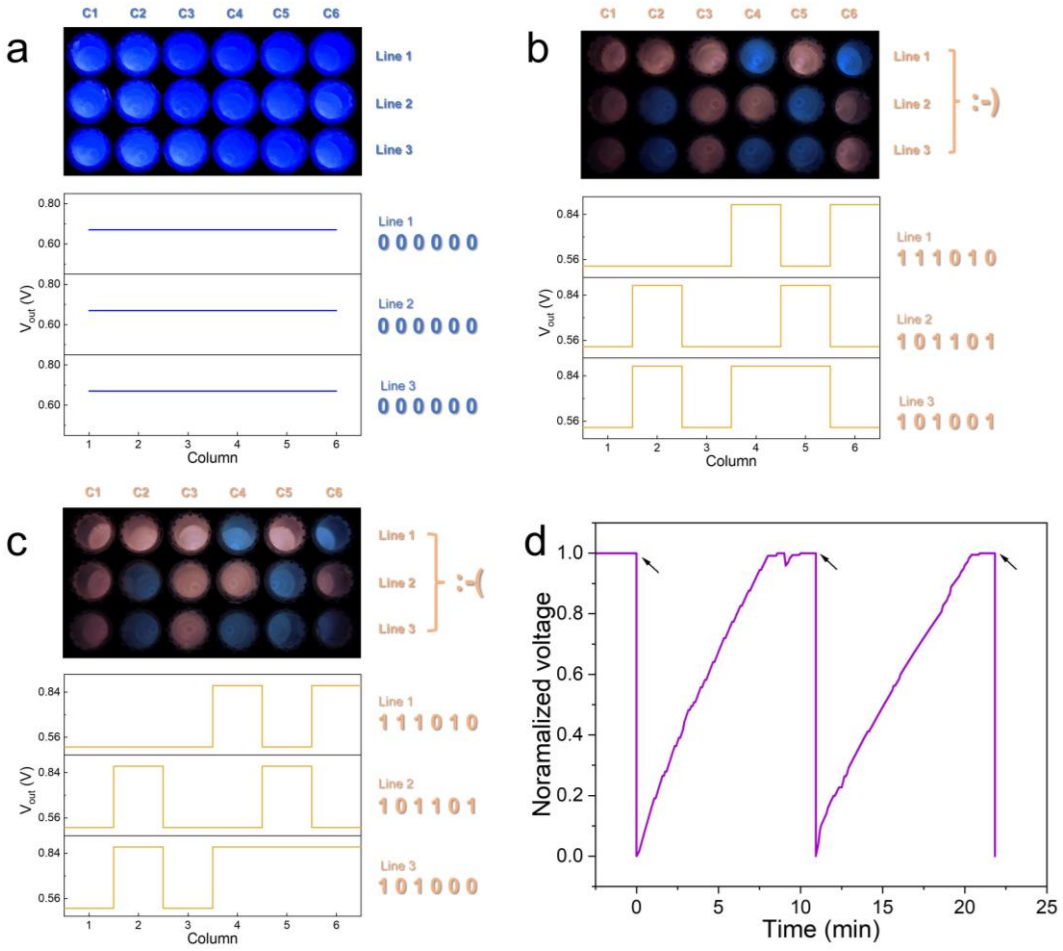

Figure S31. a-c) Storage matrix under 365 nm excitation and the corresponding voltages for each data point. The voltages can be converted into binary code to get the information. d) Time-dependent normalized voltage intensity of single data point upon several repetitive additions of ATP in the presence of 1.0 U mL^{-1} of ALP, respectively. Arrows represent the (re)fuelling points with the addition of ATP. The concentration of **1**, ATP and PB are set at 1.5×10^{-5} mol L^{-1}, 4.5×10^{-5} mol L^{-1} and 7.5×10^{-7} mol L^{-1}, respectively.

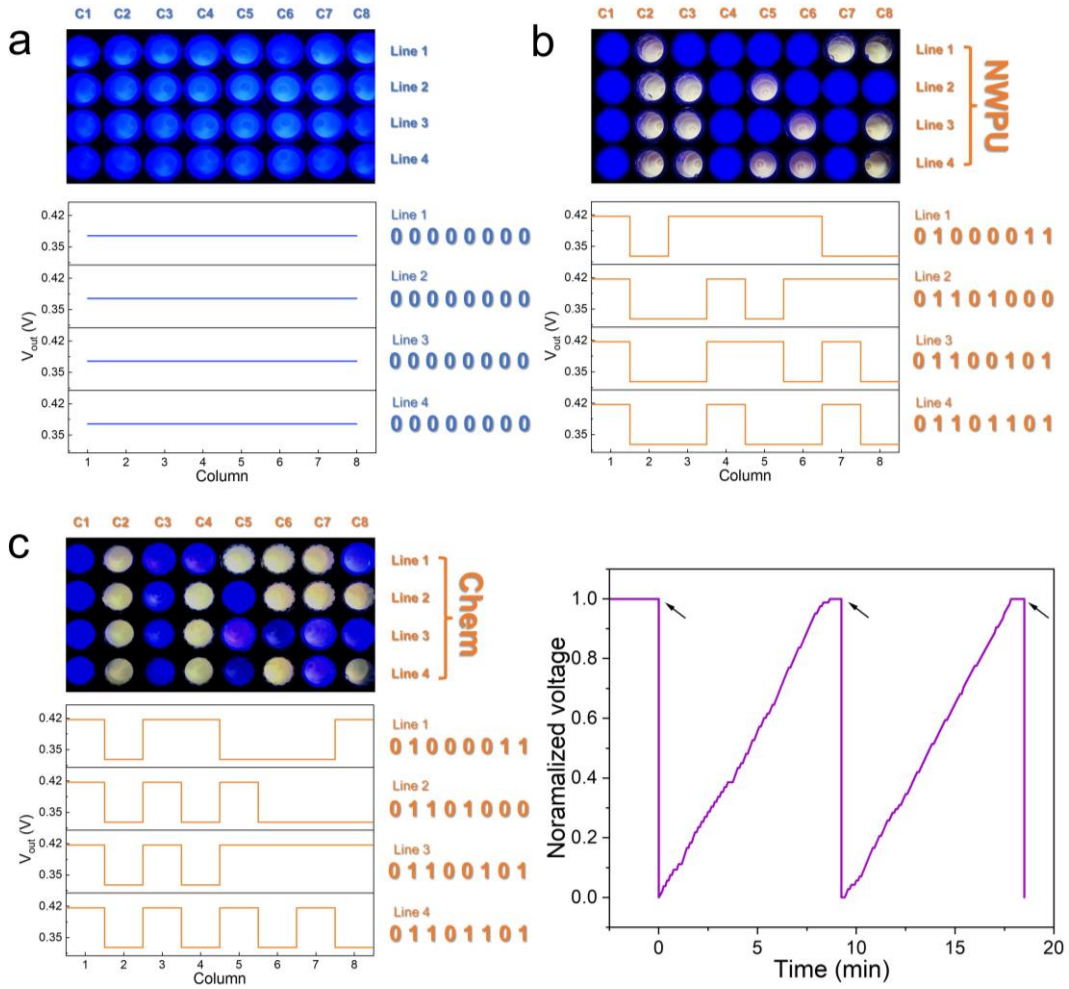

Figure S32. a-c) Storage matrix under 365 nm excitation and the corresponding voltages for each data point. The voltages can be converted into binary code to get the information. d) Time-dependent normalized voltage intensity of single data point upon several repetitive additions of ATP in the presence of 1.0 U mL^{-1} of ALP, respectively. Arrows represent the (re)fuelling points with the addition of ATP. The concentration of **1**, ATP and RhB are set at 1.5×10^{-5} mol L^{-1}, 4.5×10^{-5} mol L^{-1} and 7.5×10^{-7} mol L^{-1}, respectively.

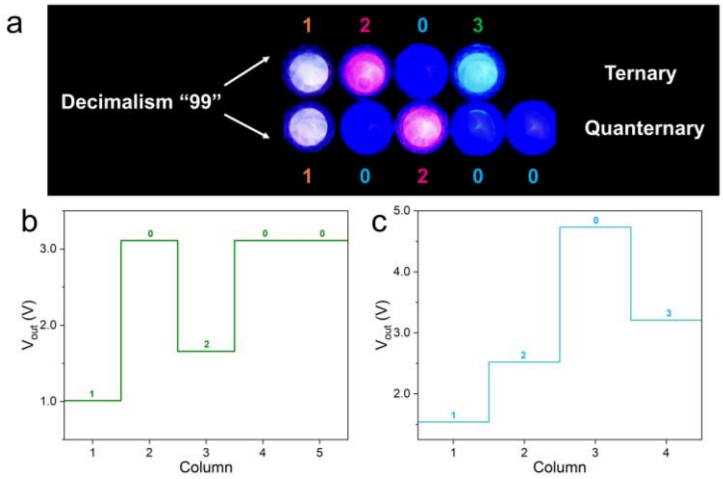

Figure S33. a) Storage matrix under 365 nm excitation with different memory level. The number "99" in decimalism can be transformed into ternary and quanternary level. b-c) The corresponding voltages for each data point in ternary and quanternary system, respectively.

6. Synthesis and Characterization

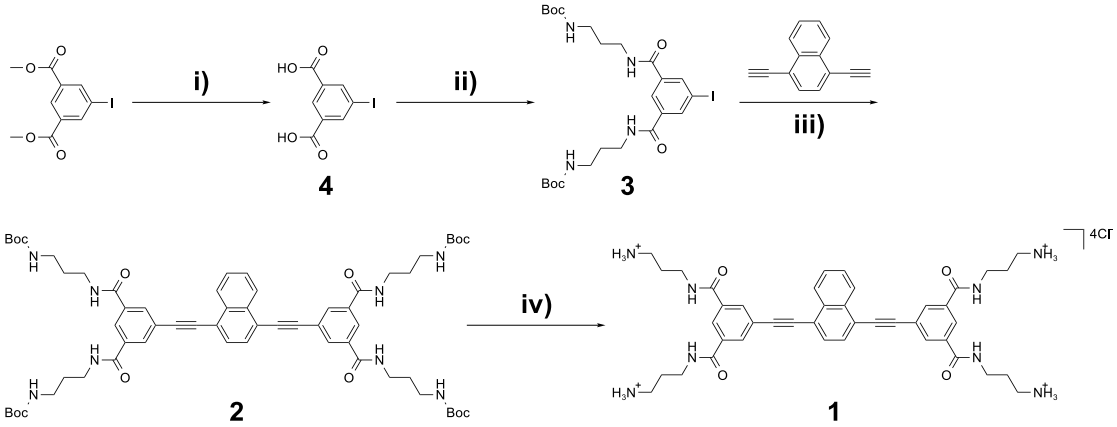

Figure S34. Synthetic routes to the targeted monomer **1**. i) NaOH, MeOH; ii) EDC, DMAP, CH_2Cl_2; iii) $Pd(PPh_3)_4$, CuI, TEA, THF; iv) HCl, dioxane.

6.1 Synthesis of compound 3

N-Boc-1,3-propanediamine (774.3 mg, 4.45 mmol), compound 4 (500 mg, 1.71 mmol), EDC (1-(3-Dimethylaminopropyl)-3-ethylcarbodiimide hydrochloride) (623 mg, 3.25 mmol) and DMAP (4-dimethylaminopyridine) (814.9 mg, 6.67 mmol) were mixed in 20 mL of CH_2Cl_2. After stirring at room temperature for 12 hours, the mixture was extracted with H_2O/CH_2Cl_2 for three times. The combined organic extracts were washed with diluted HCl for three times and dried over anhydrous Na_2SO_4, and the solvent was removed with a rotary evaporator to afford compound **3** as a white solid (889 mg, 86%). ^{1}H NMR (400 MHz, DMSO-d_6) δ (ppm): 8.61 (t, 2H), 8.24 (s, 3H), 6.79 (t, 2H), 3.20 (q, 4H), 2.92 (q, 4H), 1.58 (p, 4H), 1.33 (s, 18H). ^{13}C NMR (101 MHz, DMSO-d_6) δ (ppm): 164.34, 155.67, 137.88, 136.63, 125.90, 94.64, 77.59, 37.81, 37.27, 29.46, 28.35. ESI-MS *m*/*z*: $[M+H]^+$, $C_{24}H_{38}O_6IN_4$, calculated 605.18305; found 605.18134.

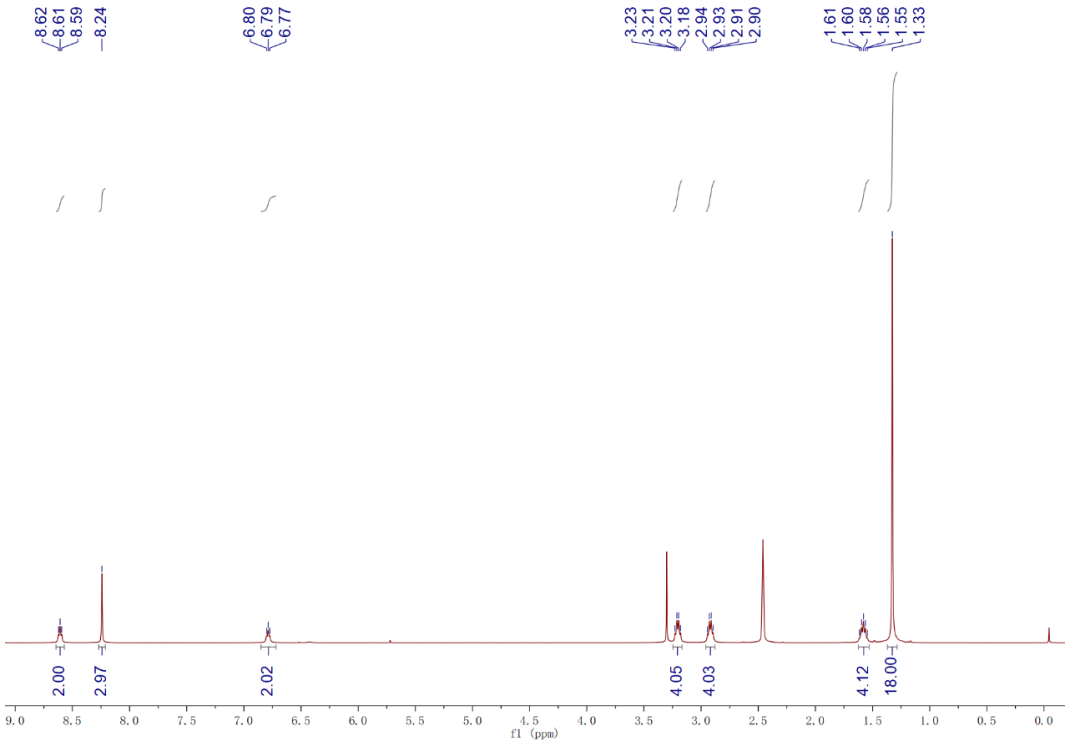

Figure S35. ^{1}H NMR spectrum (400 MHz, DMSO-d_6, 298K) of **3**.

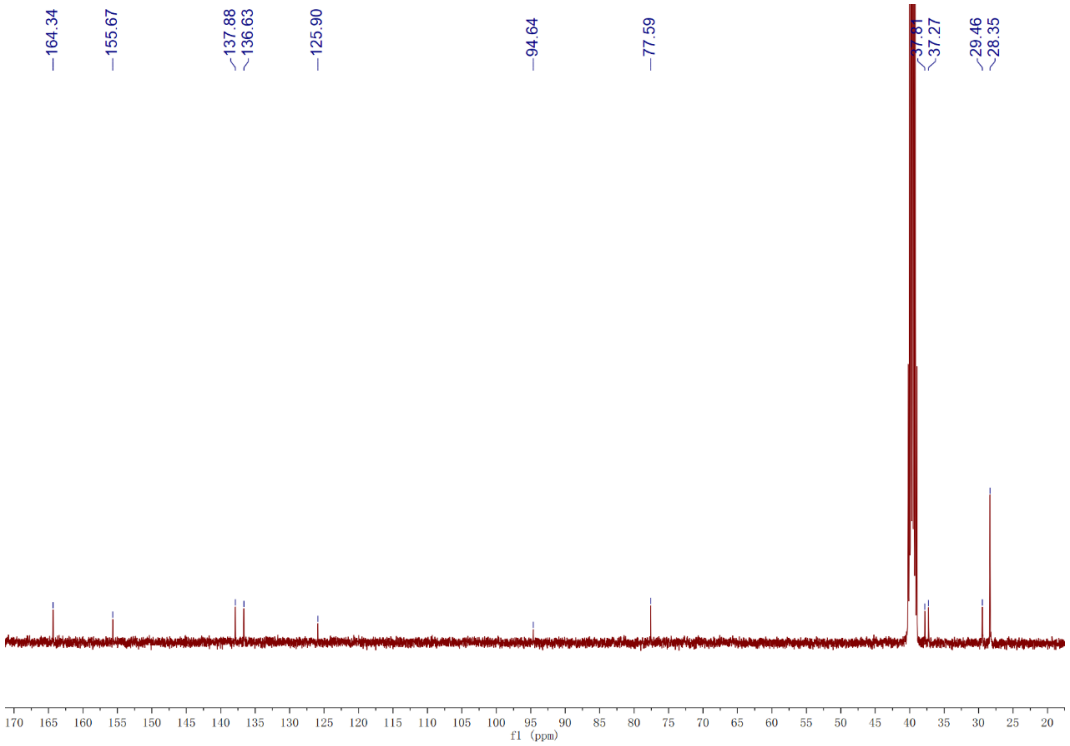

Figure S36. ^{13}C NMR spectrum (101 MHz, DMSO-d_6, 298 K) of **3**.

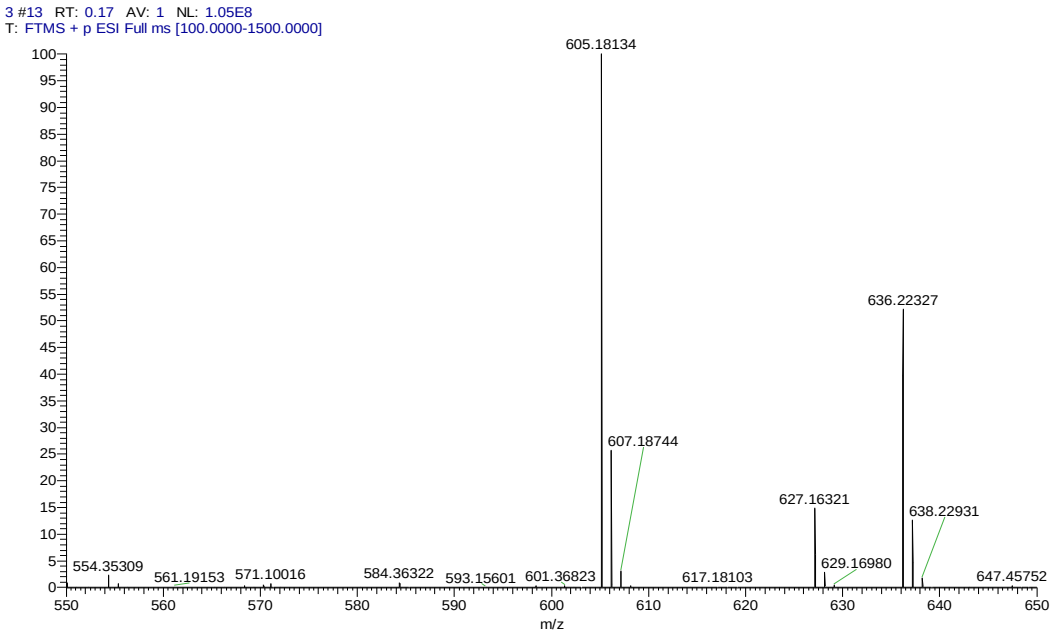

Figure S37. ESI-MS spectrum of **3**.

6.2 Synthesis of compound 2

1,4-Diethynylnaphthalene (70.0 mg, 0.40 mmol), compound **3** (556 mg, 0.92 mmol), $Pd(PPh_3)_4$ (30.0 mg, 0.04 mmol) and CuI (25.0 mg, 0.13 mmol) were mixed in 20 mL of a mixture of TEA and DMF (*v*/*v* = 1:1). After stirring at 70℃ for 22 hours, the mixture was extracted with H_2O/CH_2Cl_2 for three times. The dark-brown precipitation was then washed with CH_2Cl_2 for multiple times and dried to obtain compound **2** as an off-white solid (257.5 mg, 57%). ^{1}H NMR (400 MHz, DMSO-d_6) δ (ppm): 8.73 (t, 4H), 8.52 (dd, 2H), 8.36 (s, 2H), 8.29 (s, 4H), 7.94 (s, 2H), 7.85 (dd, 2H), 6.83 (t, J = 5.4 Hz, 4H), 3.32–3.25 (m, 8H), 3.00 (q, 8H), 1.67 (p, 8H), 1.38 (s, 36H). ^{13}C NMR (101 MHz, DMSO-d_6) δ (ppm): 164.96, 155.69, 135.56, 132.35, 130.43, 128.46, 127.08, 126.33, 122.26, 120.69, 95.26, 87.95, 77.59, 37.85, 37.31, 29.52, 28.34. ESI-MS *m*/*z*: $[M+Na]^+$, $C_{62}H_{80}O_{12}N_8Na$, calculated 1151.57879; found 1151.57678.

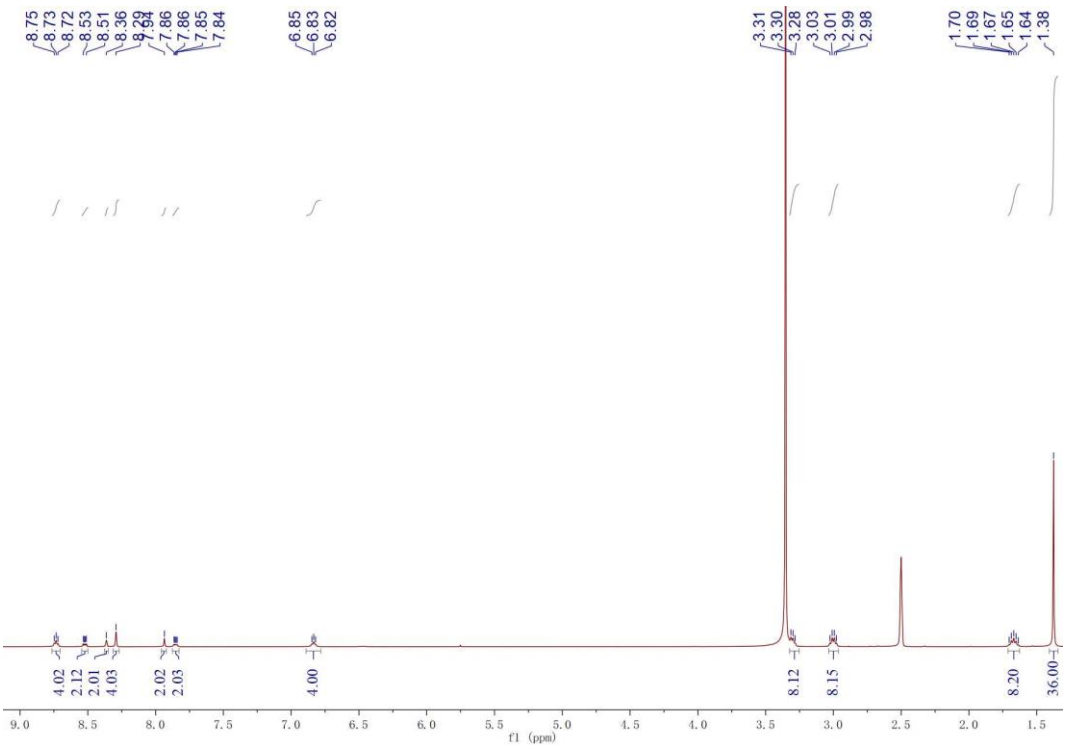

Figure S38. ^{1}H NMR spectrum (400 MHz, DMSO-d_6, 298 K) of **2**.

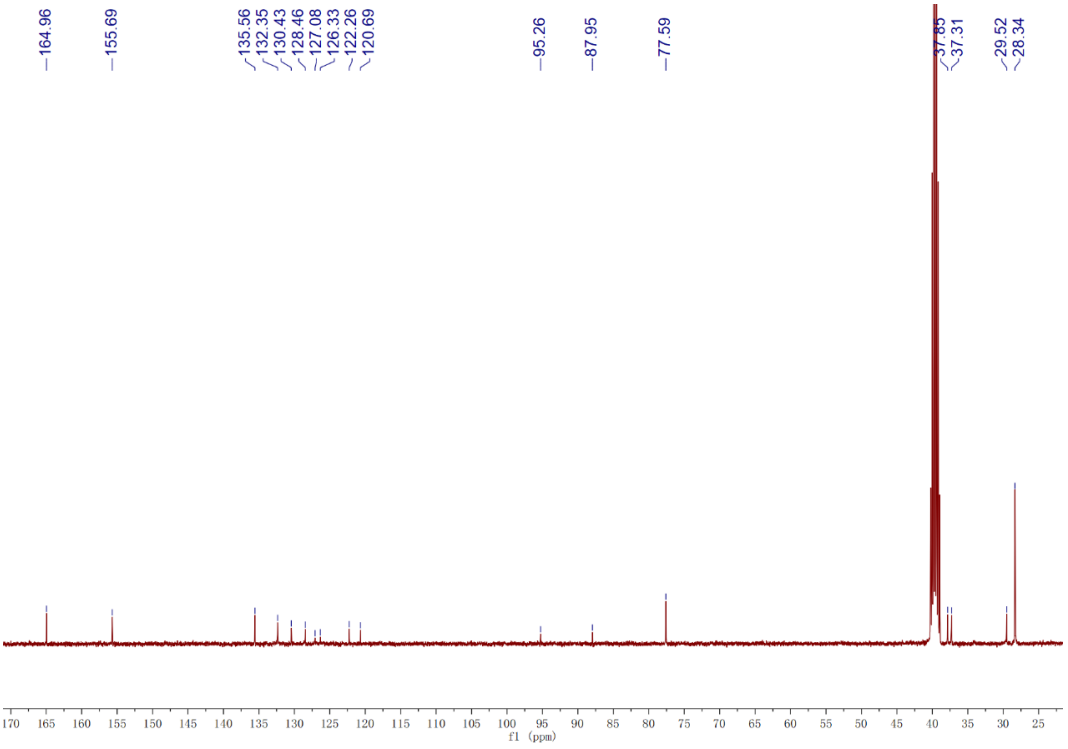

Figure S39. ^{13}C NMR spectrum (101 MHz, DMSO-d_6, 298 K) of **2**.

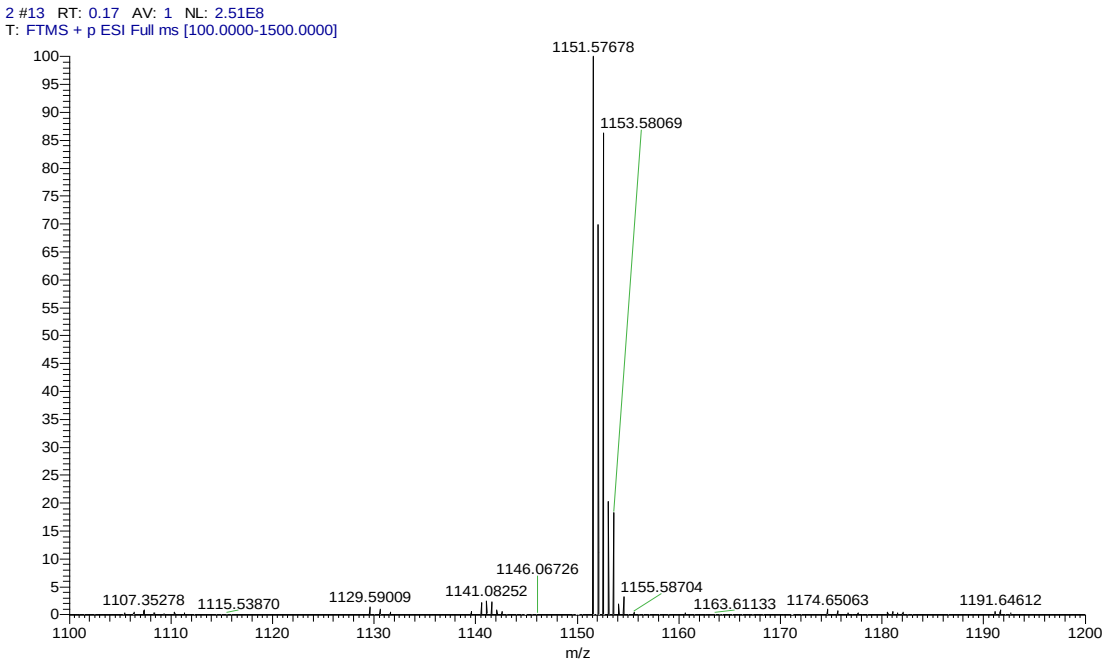

Figure S40. ESI-MS spectrum of **2**.

6.3 Synthesis of compound 1

A concentrated HCl solution was added into a dioxane (10 mL) solution of compound 2 (300 mg, 0.27 mmol) with vigorous stirring at 0 ºC under N_2 atmosphere. The mixture was allowed to warm slowly to room temperature and stirred for 24 h. The yellow precipitation was then washed with dioxane for multiple times, and dry to obtain monomer **1** as a yellow solid (205.5 mg, 87%). ^{1}H NMR (400 MHz, DMSO-d_6) δ (ppm): 9.05 (t, 4H), 8.56 (dd, 2H), 8.51 (s, 2H), 8.37 (s, 4H), 7.95 (s, 2H), 7.92–7.85 (m, 10H), 2.96 – 2.85 (m, 8H), 1.87 (p, 8H). ^{13}C NMR (101 MHz, D_2O/CD_3CN) δ (ppm): 166.97, 133.61, 132.12, 131.53, 129.27, 127.16, 125.03, 122.72, 119.87, 93.41, 87.90, 65.58, 36.15, 35.85, 25.76. ESI-MS *m*/*z*: $[M\text{-}4HCl+2H]^{2+}$, $C_{42}H_{50}O_4N_8$, calculated 365.19720; found 365.19669.

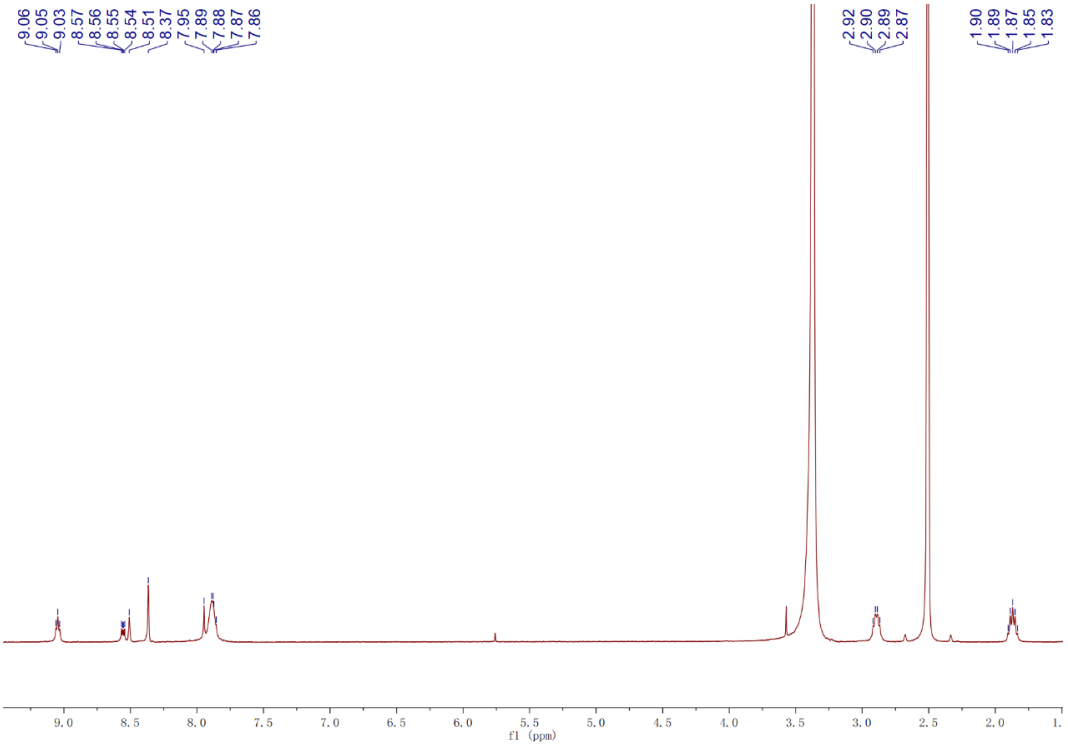

Figure S41. ^{1}H NMR spectrum (400 MHz, DMSO-d_6, 298 K) of **1**.

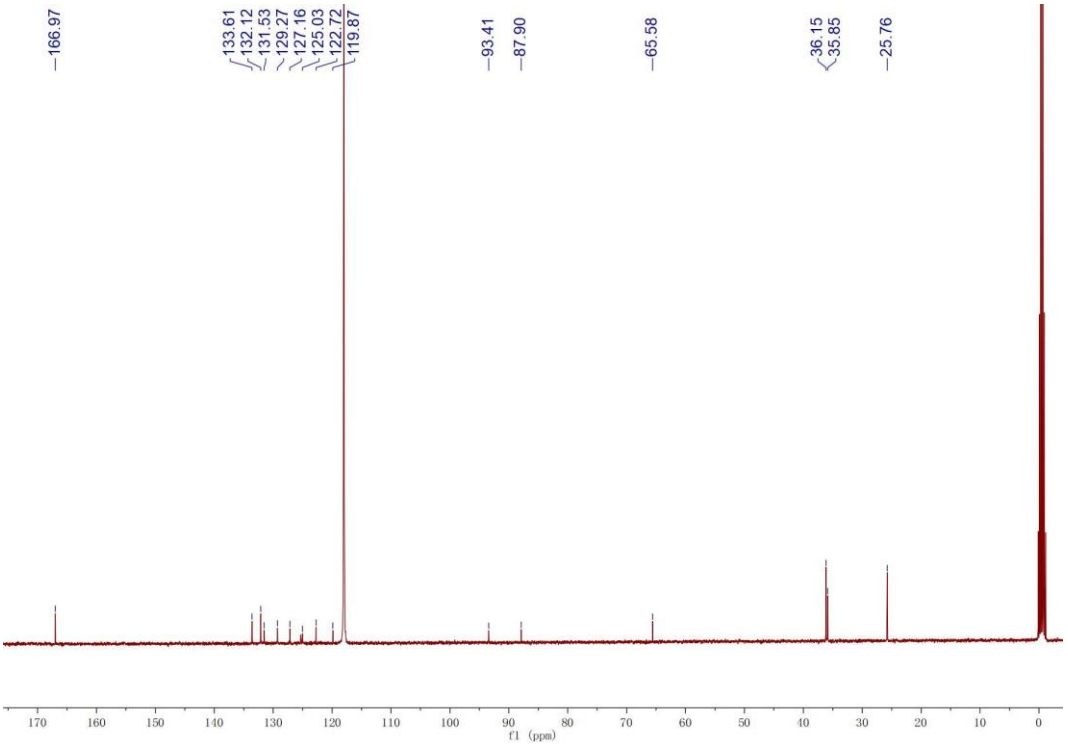

Figure S42. ^{13}C NMR spectrum (101 MHz, D_2O/CD_3CN, 298 K) of **1**.

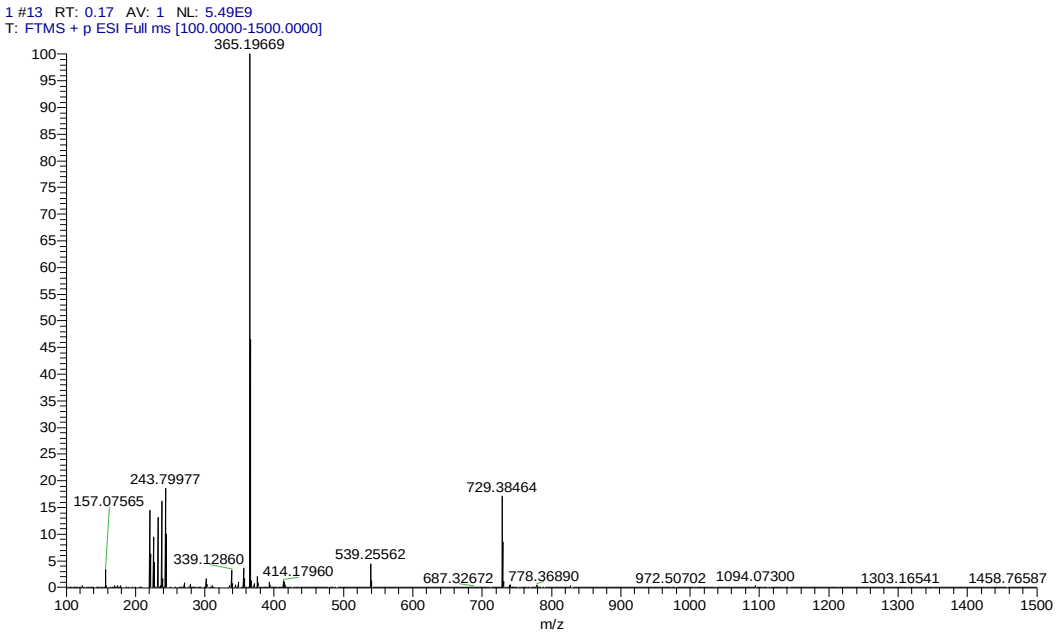

Figure S43. ESI-MS spectrum of **1**.

7. References

[S1] Y. Tanaka, R. Kawano and M. Akita, *Eur. J. Chem.*, 2022, **28**, e202201358.

[S2] K. G. Pearce and I. R. Crossley, *J. Org. Chem.*, 2020, **85**, 14697–14707.

[S3] F. Neese, *Wiley Interdiscip. Rev. Comput. Mol. Sci.*, 2022, **12**, e1606.

[S4] F. Weigend and R. Ahlrichs, *Phys. Chem. Chem. Phys.*, 2005, **7**, 3297–3305.

[S5] P. A. Korevaar, C. Schaefer, T. F. A. de Greef and E. W. Meijer, *J. Am. Chem. Soc.*, 2012, **145**, 13482 13491.

[S6] M. M. J. Smulders, M. M. L. Nieuwenhuizen, T. F. A. de Greef, P. van der Schoot, A. P. H. J. Schenning and E. W. Meijer, *Chem. Eur. J.*, 2010, **16**, 362.

[S7] A. Kumar, R. Sahaa and P. S. Mukherjee, *Chem. Sci.*, 2021, **12**, 5319.

[S8] R. S. Grynyov, A. V. Sorokin, G. Ya. Guralchuk, S. L. Yefimova, I. A. Borovoy and Y. V. Malyukin, *J. Phys. Chem. C*, 2008, **112**, 20458–20462.

[S9] P.-Z. Chen, Y.-X. Weng, L.-Y. Niu, Y.-Z. Chen, L.-Z. Wu, C.-H. Tung and Q.-Z. Yang, *Angew. Chem. Int. Ed.*, 2016, **55**, 2759–2763.

[S10] H.-Q. Peng, Y.-Z. Chen, Y. Zhao, Q.-Z. Yang, L.-Z. Wu, C.-H. Tung, L.-P. Zhang and Q.-X. Tong, *Angew. Chem. Int. Ed.*, 2012, **51**, 2088–2092.